HIGH POWER BEAM-PLASMA AMPLIFIER

Report No. 5

Fifth Quarterly Progress Report

15 December 1963 to 14 March 1964

Contract No. DA-36-039-AMC-00076(E)

Task No. 7776-10-331-28

U. S. Army Electronics Laboratories
Fort Monmouth, New Jersey

This research is part of Project DEFENDER, sponsored by the Advanced Research Projects Agency, Department of Defense.

ARPA Order No. 331-62

MICROWAVE ASSOCIATES, INC.

Burlington, Massachusetts

DISCLAIMER NOTICE

THIS DOCUMENT IS THE BEST QUALITY AVAILABLE.

COPY FURNISHED CONTAINED A SIGNIFICANT NUMBER OF PAGES WHICH DO NOT REPRODUCE LEGIBLY.

High Power Beam-Plasma Amplifier

Report No. 5

Contract No. DA-36-039-AMC-00076(E)

Technical Requirement No. SCL-5892

Dated 10 May 1962 (Phase . only)

Fifth Quarterly Progress Report

15 December 1963 to 14 March 1964

Prepared by:

M. A. Allen

C. S. Biechler

P. Chorney

H. S. Maddix

Approved by:

G. E. St. John

OBJECTIVE: To carry out research work leading to the development of a High Power Beam-Plasma Amplifier.

MICROWAVE ASSOCIATES, INC.
Burlington, Massachusetts

The work prepared under this contract was made possible by the support of the Advanced Research Project Agency under Order No. 331-62 through the U. S. Army Electronics Laboratories and the U. S. Army Electronics Materiel Agency.

TABLE OF CONTENTS

LIST OF ILLUSTRATIONS

PURPOSE

The purpose of this contract is to carry out research work leading to the development of a high-power beam-plasma amplifier. The design objectives of this contract are to develop a broadband amplifier with peak power output of twenty kilowatts in the frequency range 2700 to 3300 megacycles capable of operation at a 0.5 duty cycle and up to 100 microsecond pulse width. Supporting research will be carried out in the following problem areas:

A. Cathode elements

B. Plasma formation

C. RF coupler design

D. Large signal analysis of beam-plasma interaction

E. Gas types and pressure

F. Bandwidth

G. Noise

H. Fabrication and processing techniques

I. Tube life.

ABSTRACT

Efficiency predictions obtained from the large signal computer theory are given. A Langmuir probe plasma mapping vehicle is described and results given. A coupling experiment showing 20 db of coupling enhancement due to the plasma is discussed and the design of a second amplifier tube presented.

PUBLICATIONS, LECTURES, REPORTS AND CONFERENCES

Publications:

"Coupling to an Electron Beam through a Plasma" by M. A. Allen, C. Biechler, H. S. Maddix. Published in Applied Physics Letters vol. 4, No. 6, p. 107, March 15, 1964.

Conferences:

January 7, 1964 at Microwave Associates, Inc.

A review of progress with J. L. Carter, Project Engineer USAEL

February 17, 1964 at Microwave Associates, Inc.

A review of progress with J. L. Carter, Project Engineer USAEL

FACTUAL DATA

The following Sections I to VI contain the factual data part of this report.

I. INTRODUCTION

During this quarter the experimental and theoretical work discussed in the Fourth Quarterly Report was continued. The results from the coupling experiment culminated in the measurement of coupling enhancement of up to 20 db due to the presence of the plasma. These results which can be analyzed on the basis of radial density variations in the plasma are of great significance to the design of the final amplifier. This is the first experiment to give quantitative data on the coupling effect of a plasma of a diameter larger than the beam.

The construction of a plasma probing vehicle has allowed a point by point mapping of the plasma density. The wide variations measured indicate one source of the inconsistency encountered when only a fixed probe was used. The information gained from the plasma map has already proved useful in design of the plasma section and will be invaluable in designing plasma couplers for the final amplifier.

With construction of a second amplifier tube, quiet beam operation has been achieved at pressures around 2×10^{-4} torr in xenon. With the best results from the plasma study there now exists a small pressure range in which both a quiet beam and a stable plasma can be achieved. This is discussed in Sections IV and V.

Construction of a vehicle for production of a thermally ionized cesium plasma has continued. Several preliminary tests were performed on some of the components but, as yet, a cesium plasma has not been generated.

The theoretical work is discussed in Sections II and III. In particular, efficiency calculations using the large signal computer program show the importance of proper plasma position and axial density variation. Under the best conditions investigated efficiency close to 70% are predicted. These results again point out the need for an accurate map of the plasma density.

II. SMALL-SIGNAL THEORY

Modifications to be made to the computer program for the four roots of the secular equation are not yet completed this quarter. It is expected that these modifications will be completed early next quarter and that extensive computations can proceed.

In the meantime, a further study has been made of the secular equation and several useful approximation formulas have been derived which are valid over wide ranges of the parameters p and q. These are summarized below and their ranges of validity are specified.

Approximation Formulas

Recall from the last report that when the appropriate substitutions were made, the secular equation assumed the simplified form

$$\frac{g^2}{(g-1)^2\ (g^2-p)} = q \tag{II-1}$$

where

$$g = \gamma/\beta_e \tag{II-2}$$

$$p = \frac{T^2}{\beta_e^2}\ \frac{\omega^2(\omega_{pp}^2+\omega_c^2-\omega^2)}{(\omega_{pp}^2-\omega^2)\ (\omega_c^2-\omega^2)} \tag{II-3}$$

$$q = \frac{\omega^2-\omega_{pp}^2}{\omega_{pb}^2} \tag{II-4}$$

Equation (II-1) may be manipulated into various forms which yield decent approximations. These approximation formulas lead to forms which are amenable to iterative calculations for more accurate approximations.

To obtain one of our approximation formulas, we rewrite (II-1) as

$$g^2 = q\,(g-1)^2\,(g^2-p) \tag{II-5}$$

which can be rewritten further as

$$g^2 = -pq(g-1)^2\,(1-\frac{g^2}{p}) \tag{II-6}$$

The square root of (II-6) yields

$$g = \frac{\pm\sqrt{-pq}\sqrt{1-\frac{g^2}{p}}}{1 \pm\sqrt{-pq}\sqrt{1-\frac{g^2}{p}}} \tag{II-7}$$

For roots such that $|p|>>|g|^2$ we have the approximation formula directly from (II-7)

$$g \cong \frac{\pm\sqrt{-pq}}{1 \pm\sqrt{-pq}} \tag{II-8}$$

For a more accurate estimation of the roots, we may use the iterative formula, which follows directly from (II-7)

$$g_{n+1} = \frac{\pm\sqrt{-pq}\sqrt{1 - \frac{g_n^2}{p}}}{1 \pm\sqrt{-pq}\sqrt{1 - \frac{g_n^2}{p}}} \qquad \text{(II-9)}$$

where g_n is the n^{th} estimate of the root and $g_n + 1$ is the $(n + 1)^{st}$ estimate. The iteration process may be separated until a desired accuracy criterion is satisfied.

In a similar manner as used in deriving (II-8), other approximation formulas may be obtained. These are applicable for $|p| << |g|^2$, $|g| >> |$, and $|g| << |$. Those formulas are summarized in Table I. Also included are iterative formulas which may be used for more accurate determination of the roots.

With regard to the approximation formulas, some special features may be noted. In the approximation for $|p| >> |g|^2$ it is noted that

$$\sqrt{-pq} \equiv j\chi \qquad \text{(II-10)}$$

where χ is the quantity we have previously studied (First Quarterly). Thus, for this approximation, γ/β_e has the properties as previously described.

When $|p| << |g|^2$ we see that g is approximately given by the one-dimensional expression for space-charge waves on beam-plasma system. When $|g| >> |$, the roots correspond approximately to the plasma wave-guide modes found in the absence of the beam.

TABLE I

Summary of Approximation and Iteration Formulas

Validity Condition for Approximation	Approximation Formula	Iteration Formula
$\lvert p\rvert \gg \lvert g\rvert^2$	$g \approx \dfrac{\pm\sqrt{-pq}}{1 \pm \sqrt{-pq}}$	$g_{n+1} = \dfrac{\pm\sqrt{-pq}\,\sqrt{1-g_n^2/p}}{1 \pm \sqrt{-pq}\,\sqrt{1-g_n^2/p}}$
$\lvert p\rvert \ll \lvert g\rvert^2$	$g \approx 1 \pm \dfrac{1}{\sqrt{q}}$	$g_{n+1} = 1 \pm \dfrac{1}{\sqrt{q(1-p/g_n^2)}}$
$\lvert \ll \lvert g\rvert$	$g \approx \pm\sqrt{p \pm \frac{1}{q}}$	$g_{n+1} = \pm\sqrt{p \pm \dfrac{1}{q(1-1/g_n^2)}}$
$\lvert \gg \lvert g\rvert$	$g \approx \pm\sqrt{\dfrac{-pq}{1-q}}$	$g_{n+1} = \pm\sqrt{\dfrac{-pq(g_n-1)^2}{1-q(g_n-1)^2}}$

III. LARGE SIGNAL THEORY

Introductory Remarks

In this report the effect of varying the input drift region on the large signal behavior of beam plasma amplifiers will be discussed. Also to be discussed will be the effect of an interaction region containing an axially non-uniform plasma; modifications in the computer program which allow for such a non-uniform plasma will be described. Finally, expected efficiencies based on the large signal computations will be discussed for a number of cases.

Effects of Varying Input Drift Region

By varying the length of the input drift region it is possible to study the effects of the magnitude of velocity and current modulation on the beam on entering the plasma. On a small signal basis the impressed velocity modulation on a beam in a drift region decreases to zero in the first quarter space charge wavelength and in the same distance the current modulation grows to its maximum value. Thus, by choosing an appropriate initial velocity modulation followed by an appropriate length of drift region a particular set of input conditions may be set for the plasma region. The results in Figure 2 were arrived at by setting the initial velocity modulation to those values which yielded a current modulation on entering the plasma region approximately the same for all the cases studied. The drift regions were chosen in order that varying amounts of velocity modulation would be present on the beam at the input to the plasma region.

BLANK PAGE

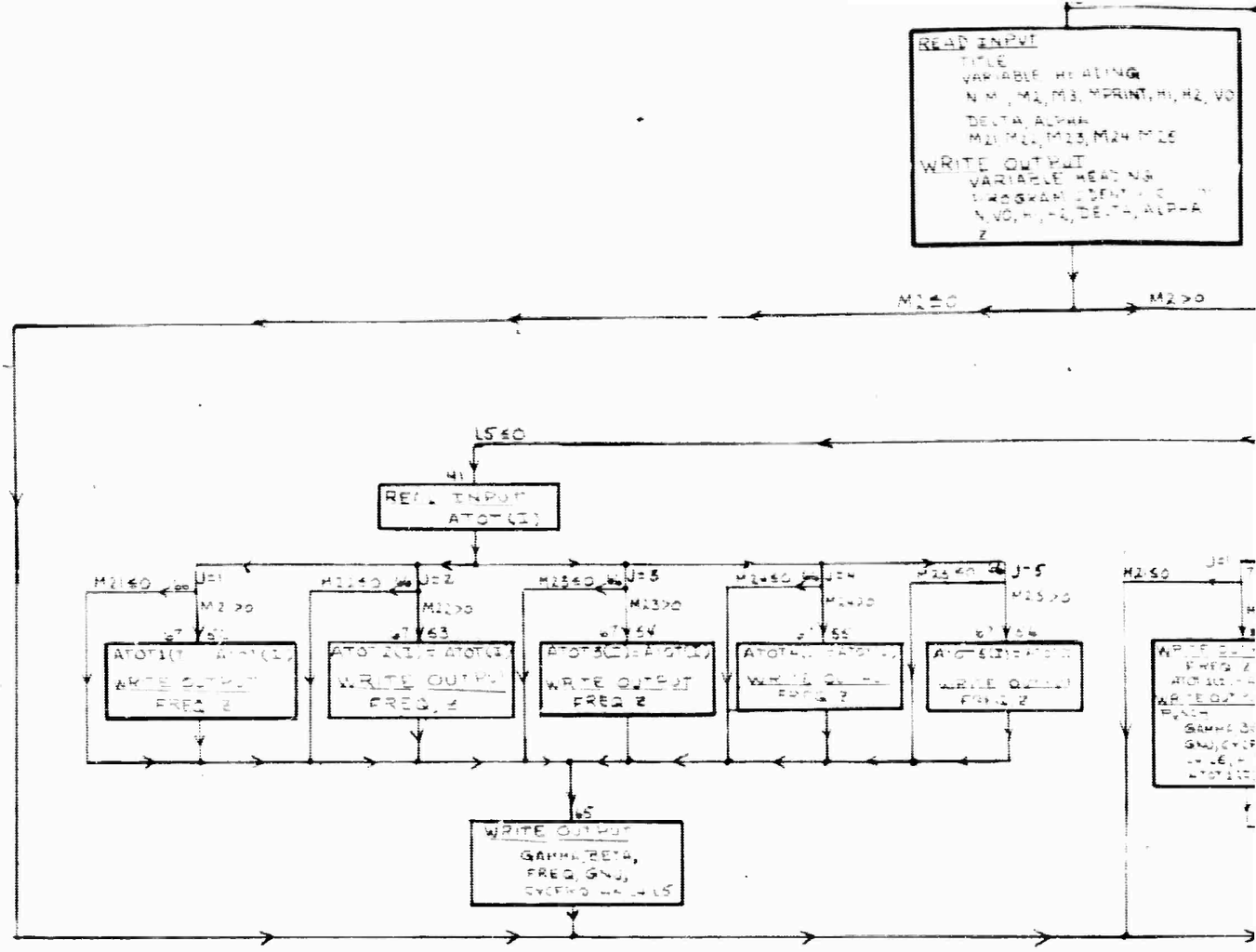
READ INPUT
TITLE
VARIABLE HEADING
M1, M2, M3, MPRINT, H1, H2, V0
DELTA, ALPHA
M11, M12, M13, M14, M15
WRITE OUTPUT
VARIABLE HEADING
M1, M2, M3, MPRINT, H1, H2, V0, DELTA, ALPHA
M2≤0
M2>0
L5≤0
READ INPUT
ATOT(I)
M2≤0
M2>0
M2≤0
M2>0
M2≤0
M2>0
M2≤0
M2>0
J=5
M2≤0
M2>0
WRITE OUTPUT
FREQ, Z
WRITE OUTPUT
FREQ, Z
WRITE OUTPUT
FREQ, Z
WRITE OUTPUT
FREQ, Z
WRITE OUTPUT
GAMMA, BETA,
FREQ, GNU,

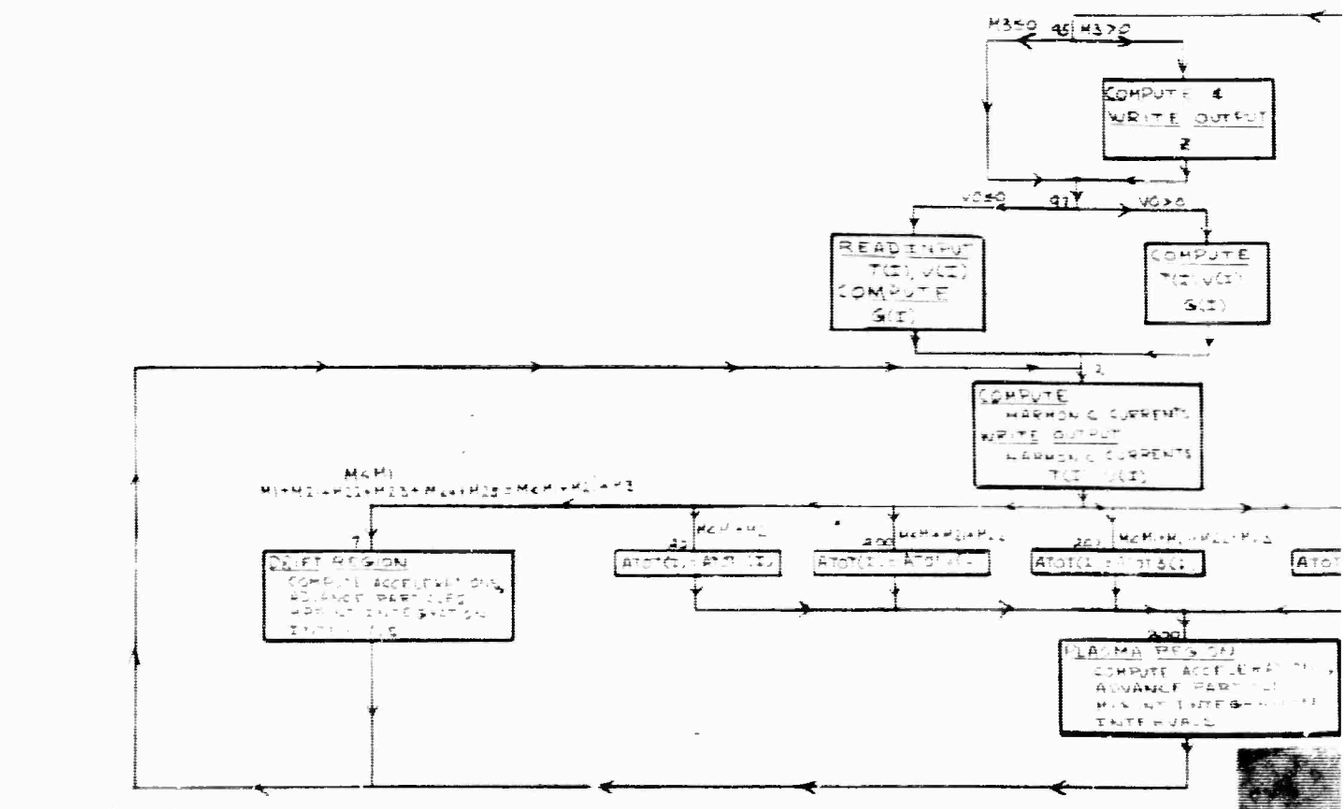
M3≤0
M3>0
COMPUTE
WRITE OUTPUT
Z
V0≤0
V0>0
READ INPUT
T(I), V(I)
COMPUTE
G(I)
COMPUTE
G(I)
COMPUTE
WRITE OUTPUT
T(I), V(I)
M≤M1
M1+M2+M11+M12+M13+M14+M15=M≤M+M2+M3
DRIFT REGION
PLASMA REGION

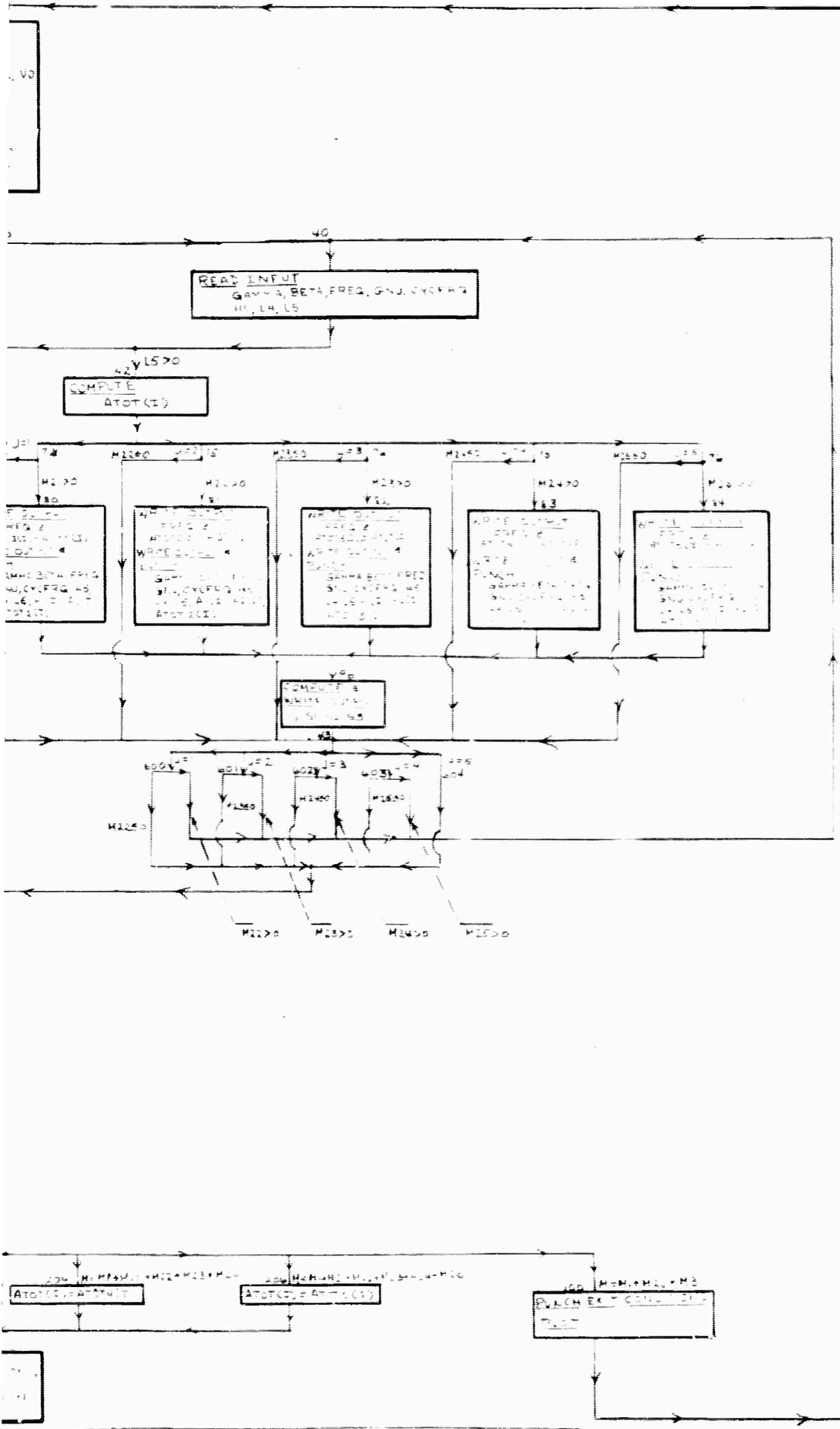

FIGURE 1

COMPUTER FLOW CHART FOR AXIAL PLASMA VARIATIONS

FIGURE 2

FUNDAMENTAL CURRENT VS. DISTANCE (PLASMA REGION BETWEEN ARROWS)

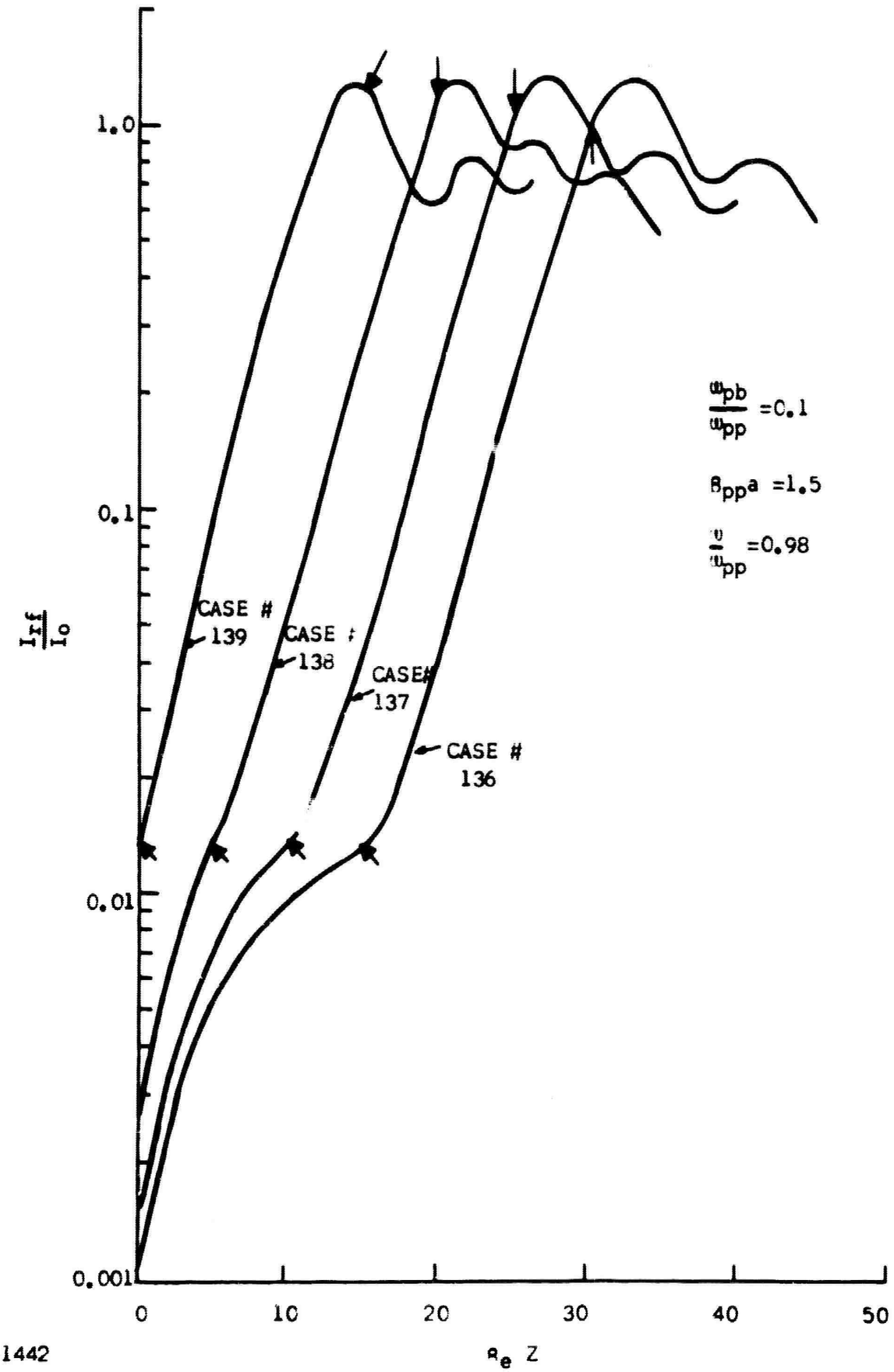

D-1442

Case 136 has a first drift region which is close to a quarter space charge wavelength and there the beam enters the plasma with the least amount of velocity modulation. For cases 137-139 the beam is increasingly velocity modulated as it enters the plasma region. In all cases the beam enters the plasma with approximately the same current modulation. Figure 2 shows how the fundamental component of the RF current grows as a function of distance down the tube. It is noted that for all cases the current modulation grows in the plasma at approximately the same rate, to the same maximum values. However the depth of velocity modulation at the point of maximum current bunching is different for the cases studied. In this large signal analysis we are following the trajectories of 32 electron disks. In Figures 3-6 the velocities of all 32 disks in an RF cycle at the plane of maximum bunching are plotted as a function of the transit time across this plane. It is seen that the velocity spread at the point of maximum bunching depends on the input drift length. In Figure 3 most of the electron velocities lie within 25% of the dc beam velocity, while in Figure 6 this condition is only true for velocities within 50% of the dc velocity. It is concluded that for efficient operation, assuming a resonant cavity output, the input drift distance should be set to give minimum velocity modulation on entering the plasma region.

Axially Non-uniform Plasma

The computer program was modified to allow the treatment of an axially non-uniform plasma. Figure 1 shows the flow diagram for the modified program. It is seen that the plasma region can be divided

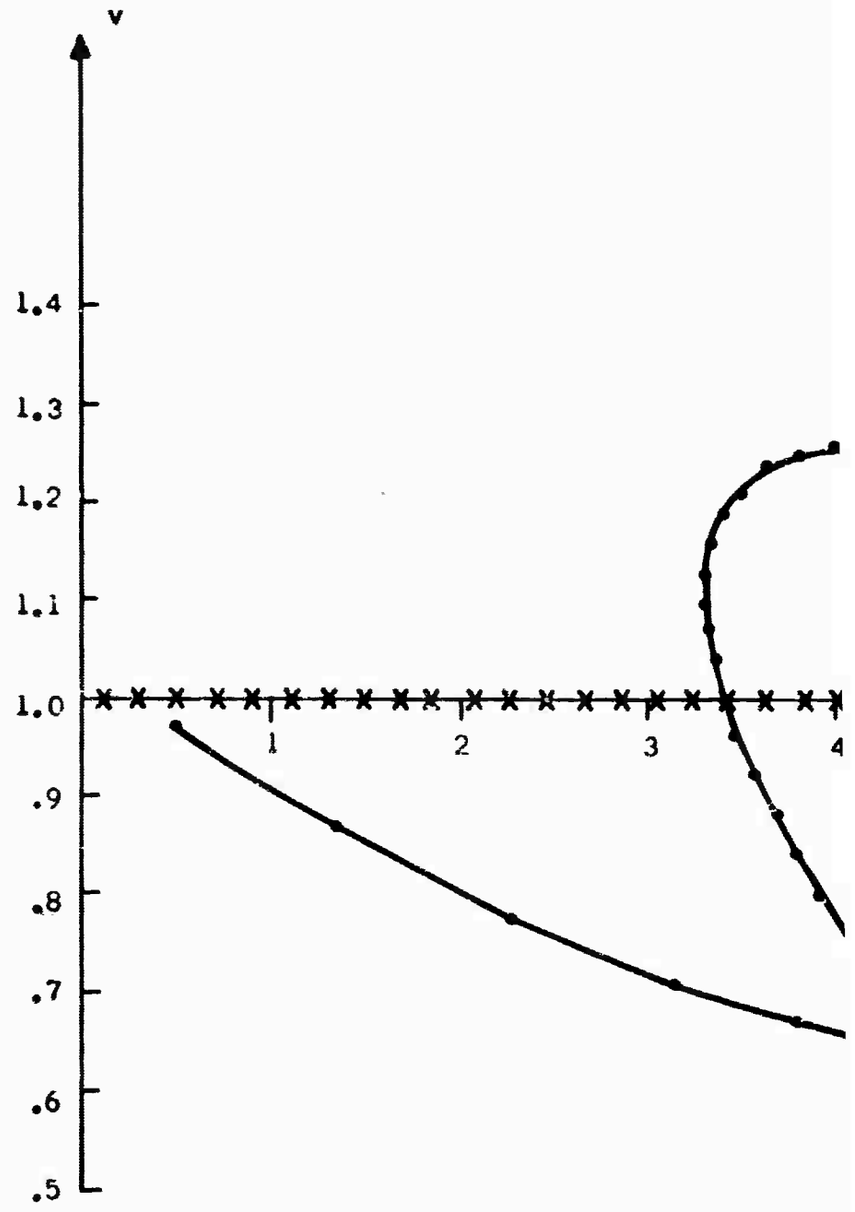

D-1441

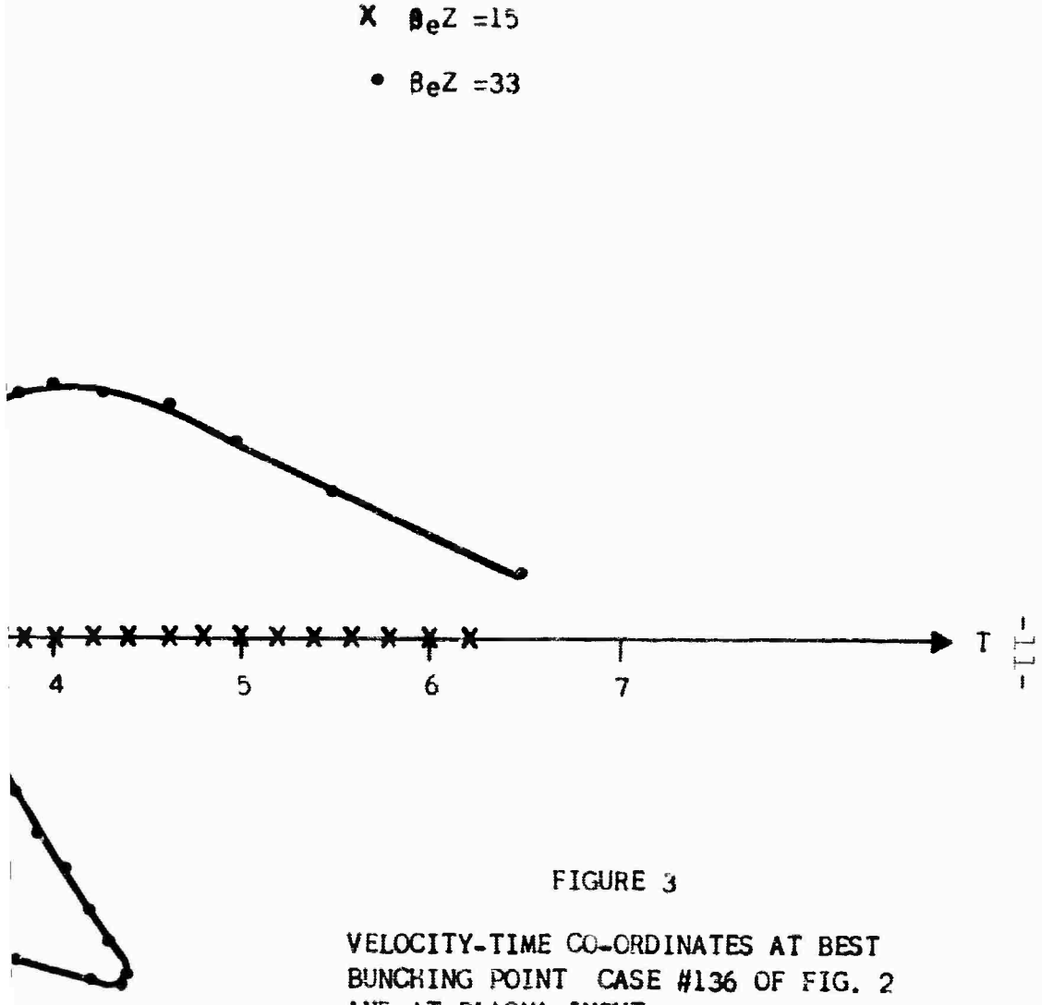

FIGURE 3

VELOCITY-TIME CO-ORDINATES AT BEST BUNCHING POINT CASE #136 OF FIG. 2 AND AT PLASMA INPUT

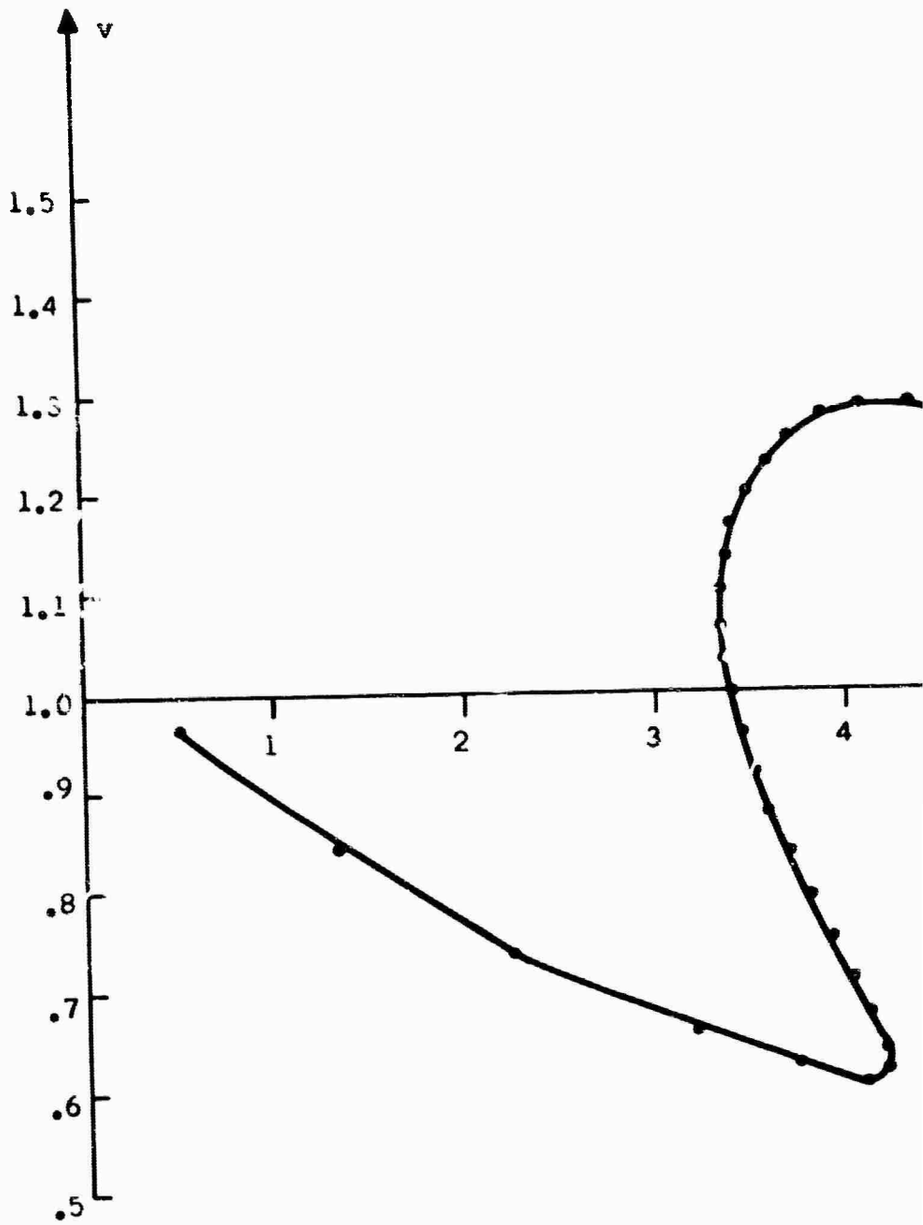

D-1440

• $B_e Z = 27$

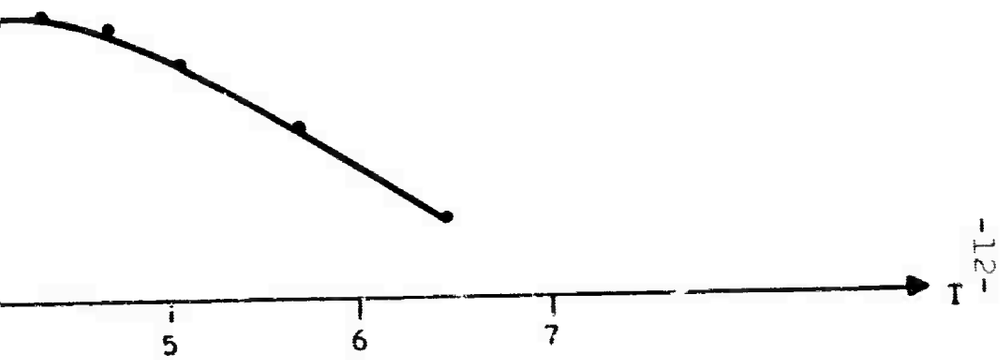

FIGURE 4

CASE #137 OF FIG. 2

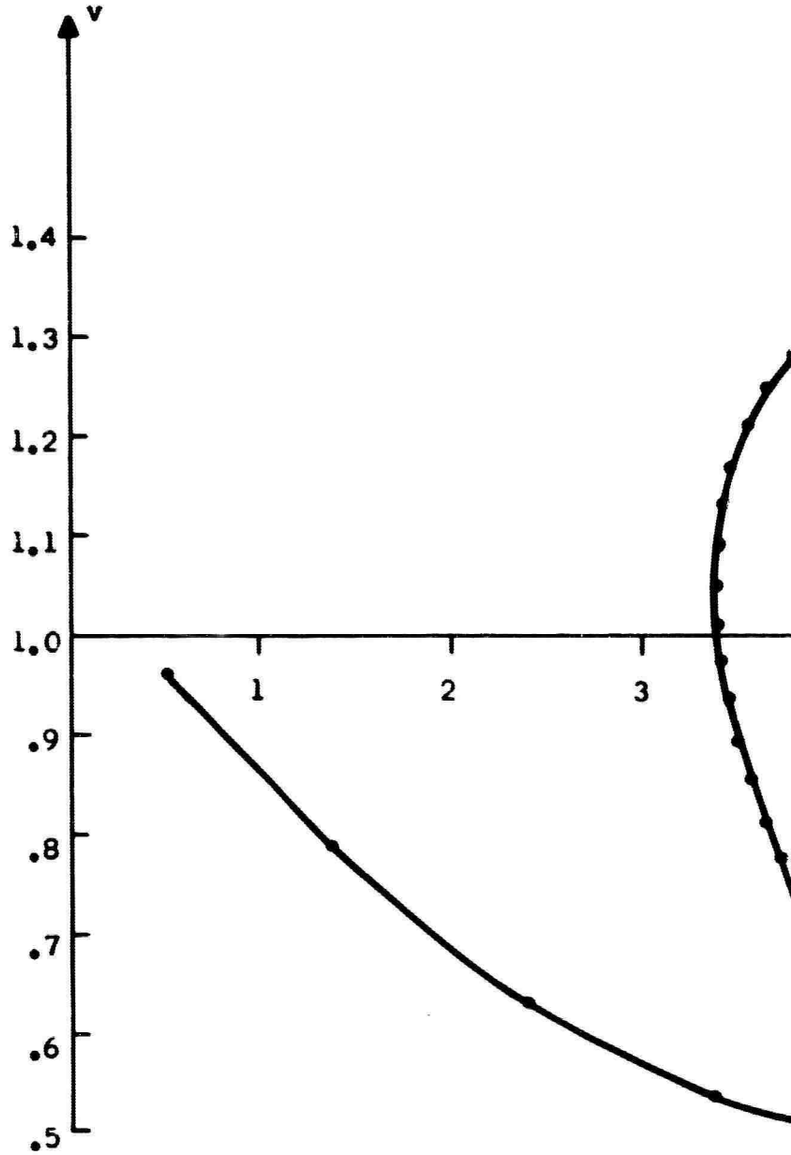

D-1438

• $\beta eZ = 21$

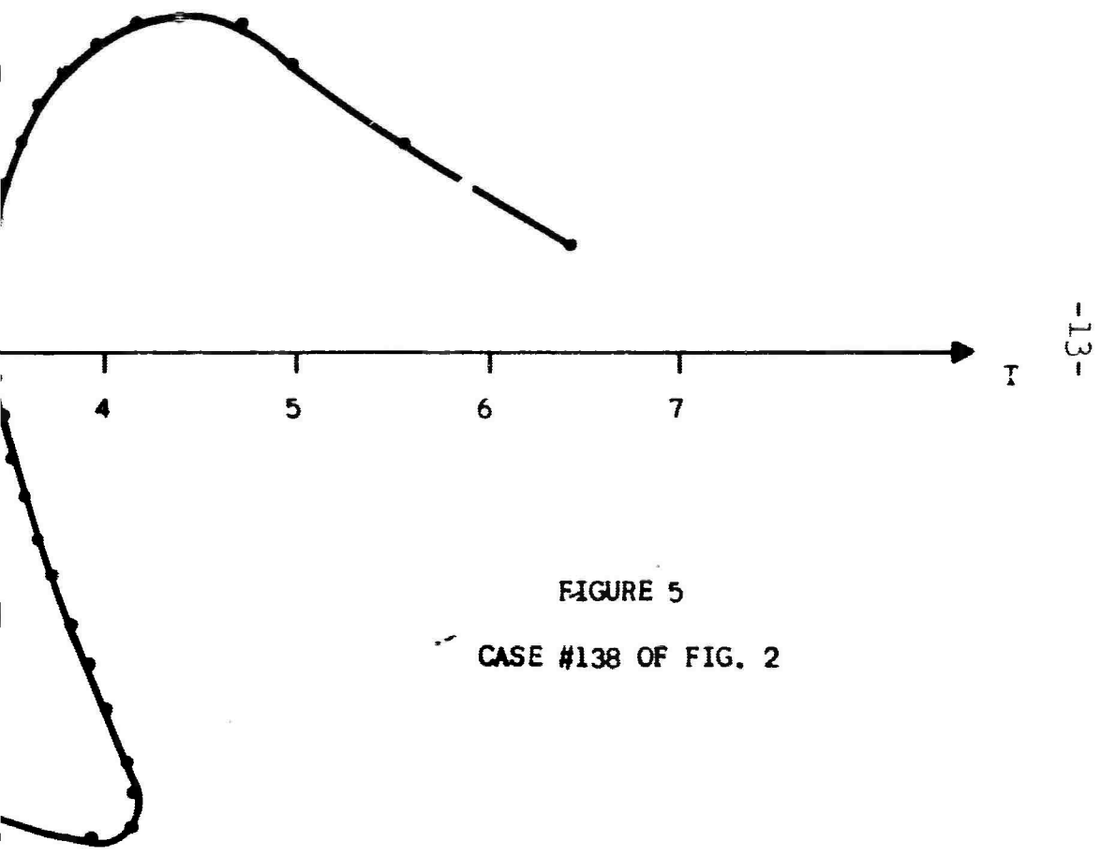

FIGURE 5

CASE #138 OF FIG. 2

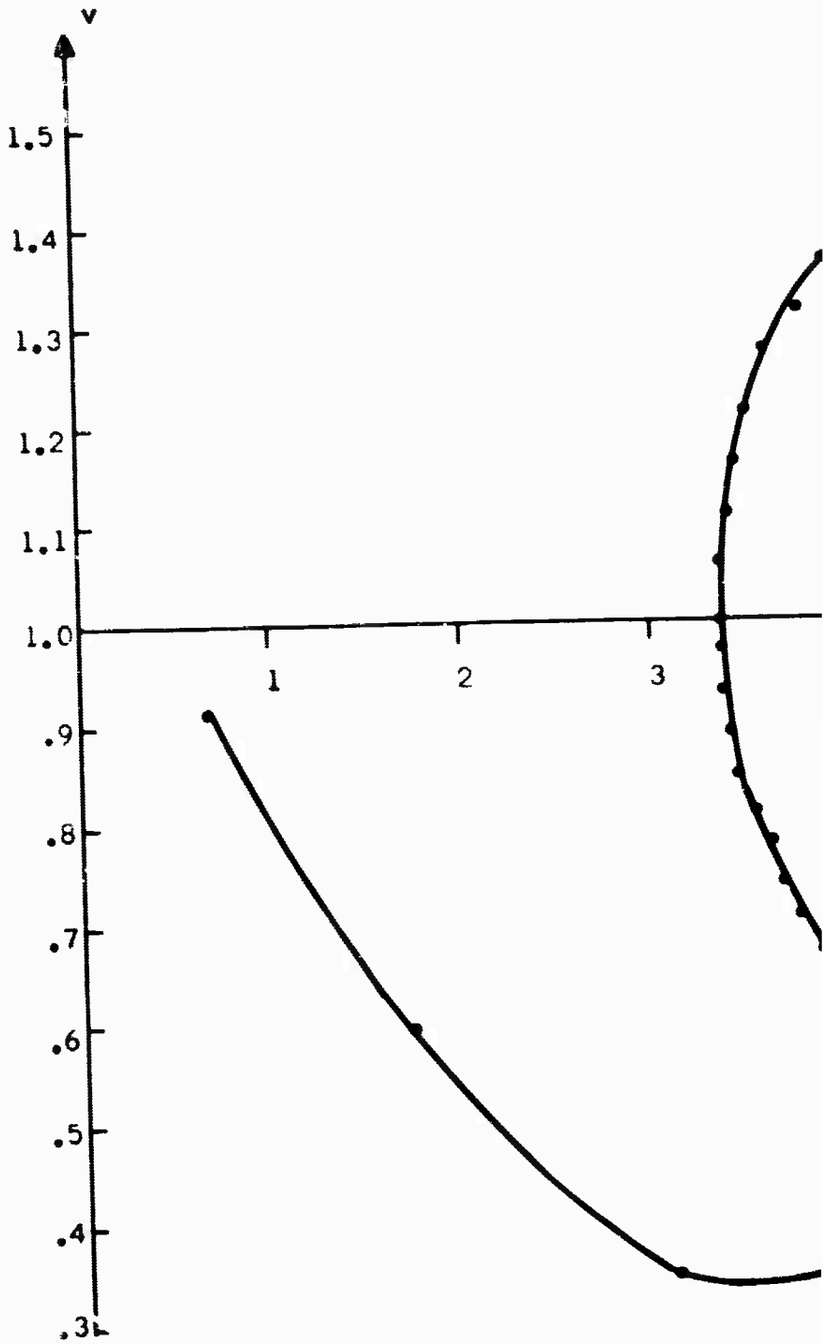

D-1439

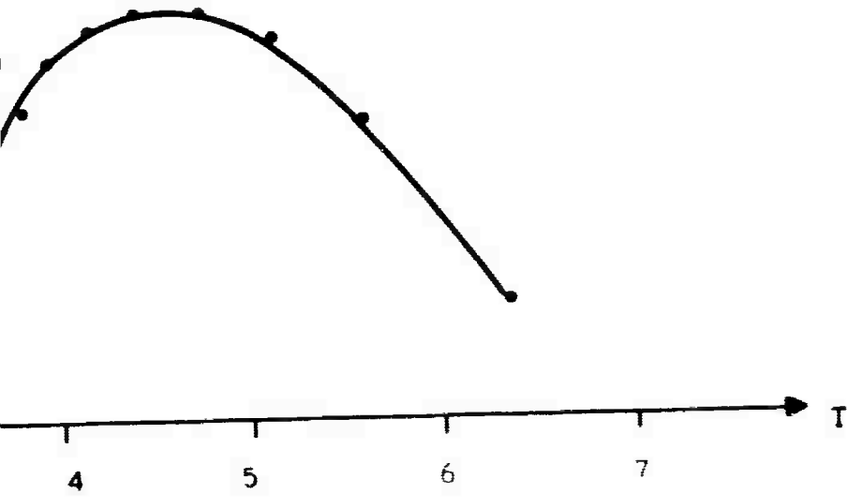

FIGURE 6

CASE #139 OF FIG. 2

up into a maximum of five regions in which the ratio between the plasma density and the applied frequency may be different. In a practical plasma generator which would be employed in the experimental tubes, axially non-uniform plasma densities are expected, and indeed are desirable to attain appreciable bandwidths. It is thus necessary to investigate operation of the beam plasma amplifier with axially non-uniform plasmas. In the case whose results are plotted in Figure 7 there is a plasma region of high density skirted by lower density regions at the input and output ends. Thus for a fixed frequency f, the ratio f/f_r is higher at the input and output ends of the plasma. For the case chosen, ratios of fundamental current to dc beam current of over 1.3 were obtained. It can be seen from Figure 8 that, at the point of maximum bunching, the velocity spread of most of the electrons close to the center of the bunch is less than 15% of the dc velocity indicating efficient operation with the cavity couplers. It is noted from Figure 9 that the velocity spread increases rapidly with distance from the maximum bunching point in the second drift region indicating that the position of the output coupler for efficient operation is critical.

Efficiency Considerations

In calculating the conversion efficiency, η it is necessary to include the magnitude of the current bunching, the allowable voltage swing at the output gap and the circuit efficiency of the output coupler[1].

1. S. E. Webber, "Ballistic Analysis of a Two-Cavity Finite Beam Klystron," I.R.E. Trans. PGED, vol. ED-5, pp. 98; April 1958.

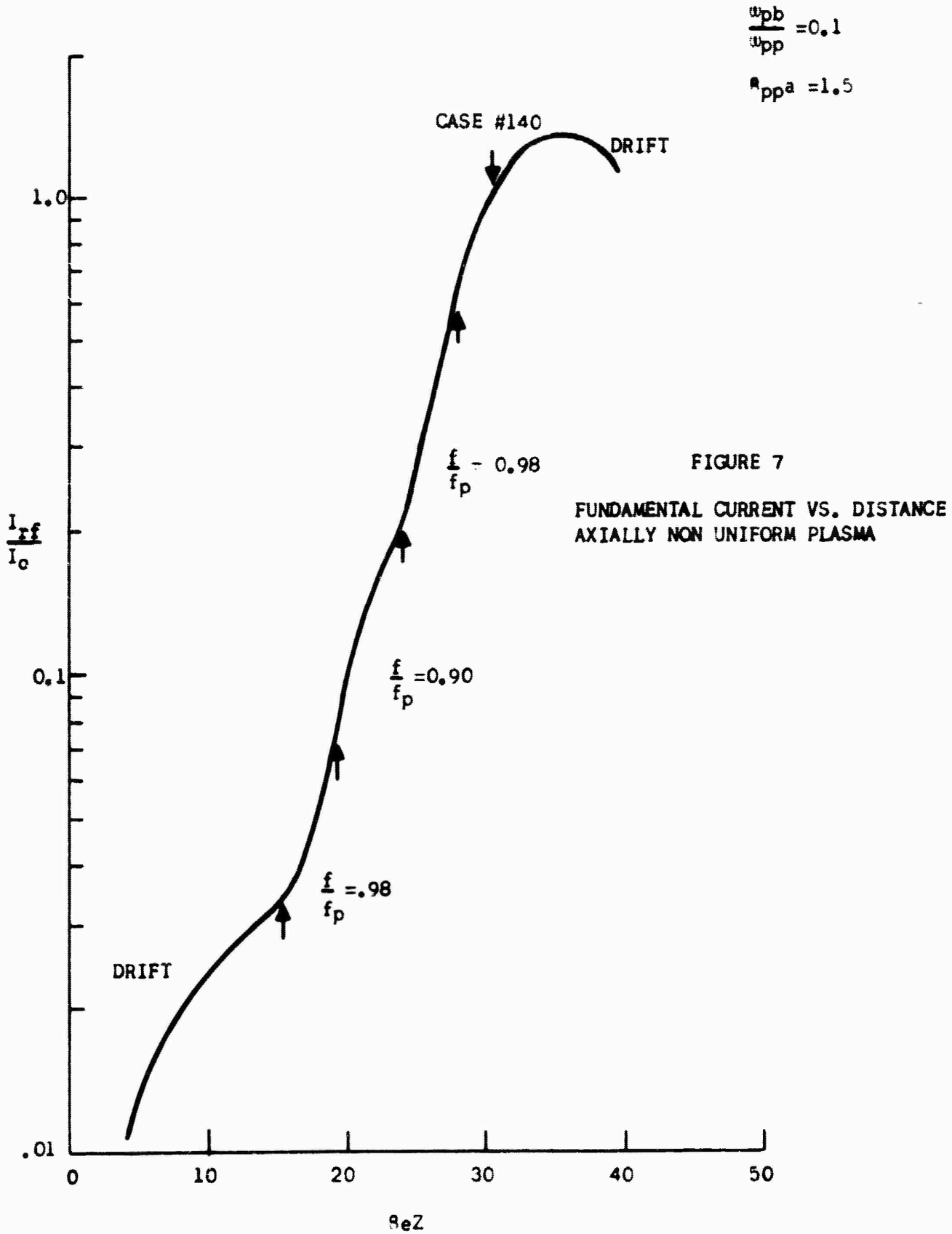

FIGURE 7

FUNDAMENTAL CURRENT VS. DISTANCE
AXIALLY NON UNIFORM PLASMA

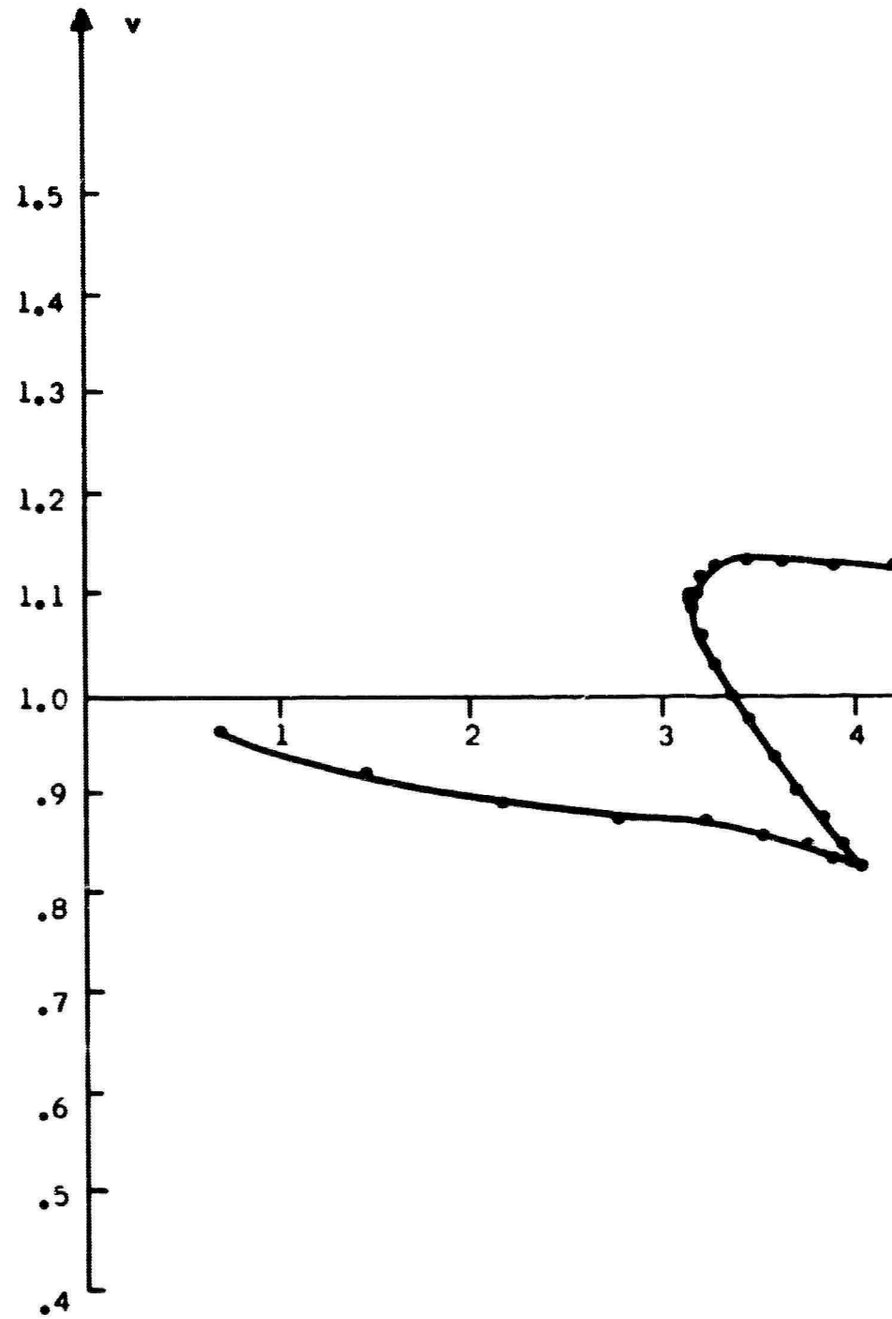

D-1436

• BeZ = 35.00

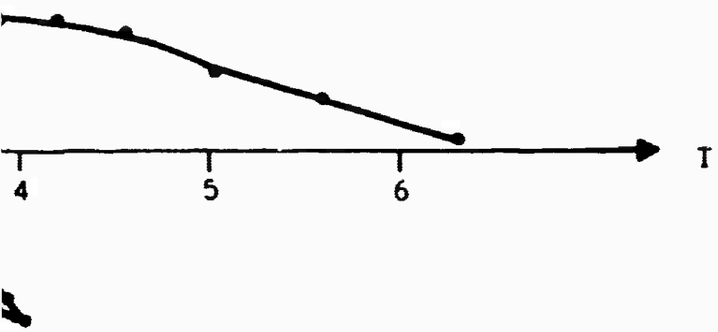

FIGURE 8

VELOCITY-TIME CO-ORDINATES AT BEST BUNCHING POINT SAME CASE AS FIG. 7

CASE #140

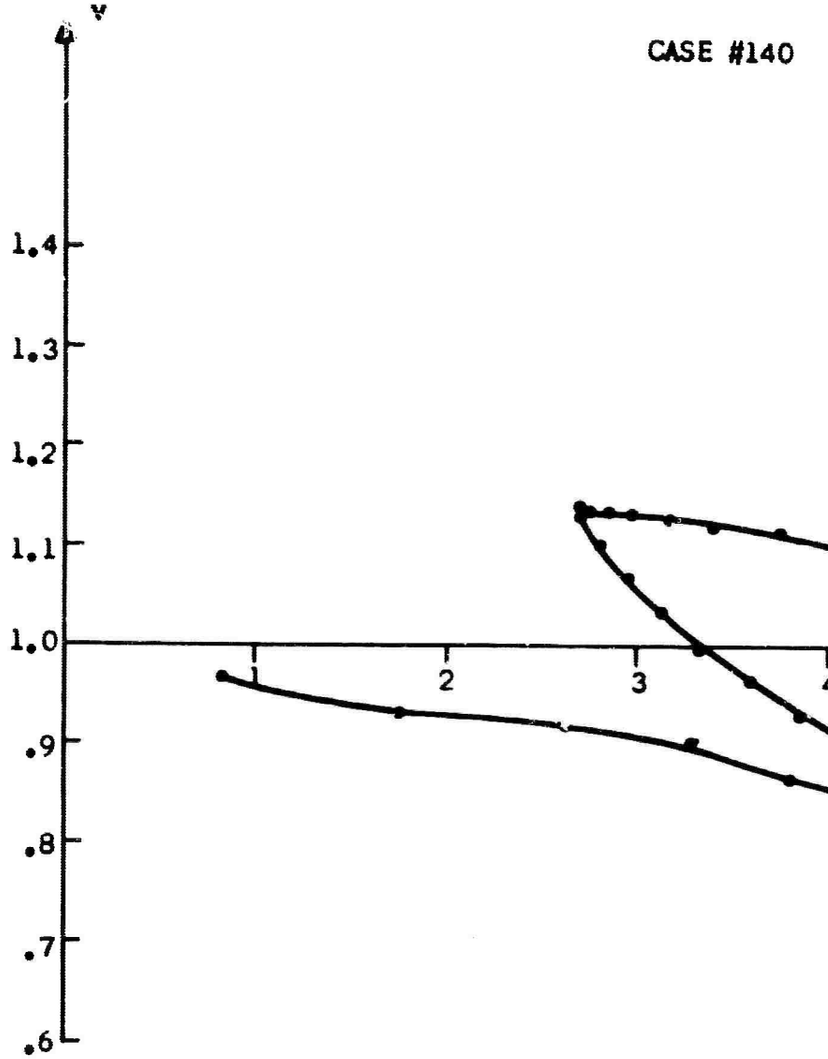

D-1435

40 • R_eZ = 3900

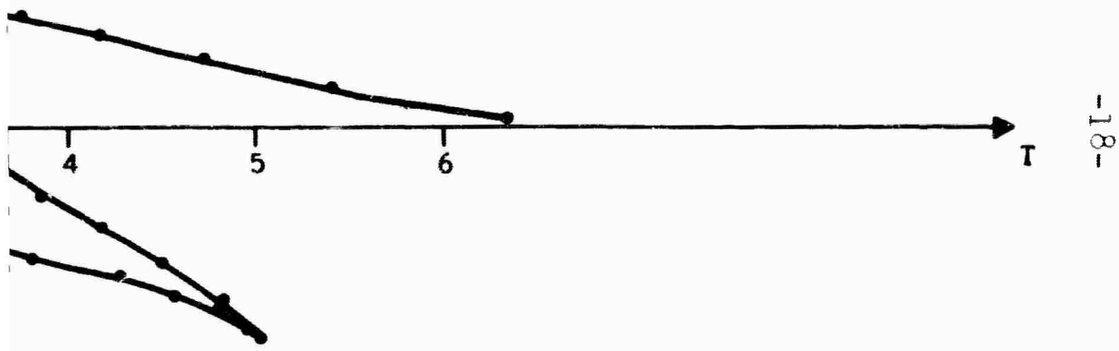

FIGURE 9

VELOCITY-TIME CO-ORDINATES AT POSITION
IN TUBE PART THE BEST BUNCHING POINT
FOR SAME CASE AS FIG. 7

$$\eta = 1/2 \; (I_{rf}/I_o) \; (V_{rf}/V_o) \; (\eta_{ce})$$

V_{rf} is the amplitude of the voltage swing at the output gap, V_o is the dc beam voltage.

We will consider the case of a circuit efficiency of 100%. The expressions for I_{rf}/I_o will be that obtained from the large signal theory and the value for the effective RF voltage swing will be taken about 10% above the value necessary to slow down to zero velocity the slowest electron at the plane of maximum bunching.

Referring to Figures 7 and 8, the conversion efficiency for an output gap placed at the position of maximum bunching for the axially non-uniform plasma considered is given by

$$\eta = 1/2 \times 1.32 \times (1.05)^2$$

that is, η approximately equals 70%. We conclude that, from the conditions chosen for this non-uniform plasma, given a suitable output coupling circuit then very high efficiencies are predicted for the beam-plasma interaction.

Considering the cases studied previously with varying input drift distances it is instructive to see the large differences in conversion efficiency obtainable with these different input conditions. Referring to Figure 2 and 3, the conversion efficiency for the point of maximum bunching for case 136, is given by

$$\eta = 1/2 \times 1.3 \times (.9)^8$$

that is, η approximately equals 53%. Referring now to case 139, the conversion efficiency is now given by

$$\eta = 1/2 \times 1.3 \times (.7)^8$$

that is η equals approximately 32%. Thus it is seen that at least for conventional couplers, both the placing of the plasma with respect to the input drift region and its density variation are critical when high efficiencies are desired. However, this does not necessarily apply to the case of coupling through the plasma as is described in the following section. The detailed mechanism whereby the amount of velocity spread on the beam affects the conversion of space-charge wave energy to electromagnetic energy through the plasma modes is not yet understood and is under current investigation.

Plans for Next Quarter

Further investigation of the detailed effects of saturation and efficiency will be carried out.

IV. PLASMA GENERATION

During this report period, emphasis was placed on obtaining reliable Langmuir probe data to provide an electron density distribution within the plasma section. The effects of different grid configurations, as well as different circuit arrangements were also investigated in conjunction with the density measurements. In addition, various inert gases were examined to determine if other gases besides xenon could provide the requisite density of 1.1×10^{11} electrons/cm^3 at a pressure below that at which beam break-up occurs. The investigations of thermally ionized cesium plasmas was continued.

The basic electrode structure investigated during this period is shown in Figure 10. This structure is similar to that reported in the previous quarterly report, with the exception that the grid close to the lower cathode has been eliminated. The reason for eliminating only one of the close grids was to provide a controlled environment for determining plasma generator behavior with and without the close grids. This can be realized by operating the tube alternately with circuits A and B in Figure 11. In both cases, the circuits are operated with only one cathode hot. In circuit A, the close grid (G_1) is tied to a cold cathode (R) and we have essentially a three element tube, inasmuch as the close grid and the cold cathode act as a common electron reflector. This arrangement effectively eliminates any influence of G_1 on the discharge. In circuit B we have a four element tube; a hot cathode (K), a cold cathode (R), and two grids

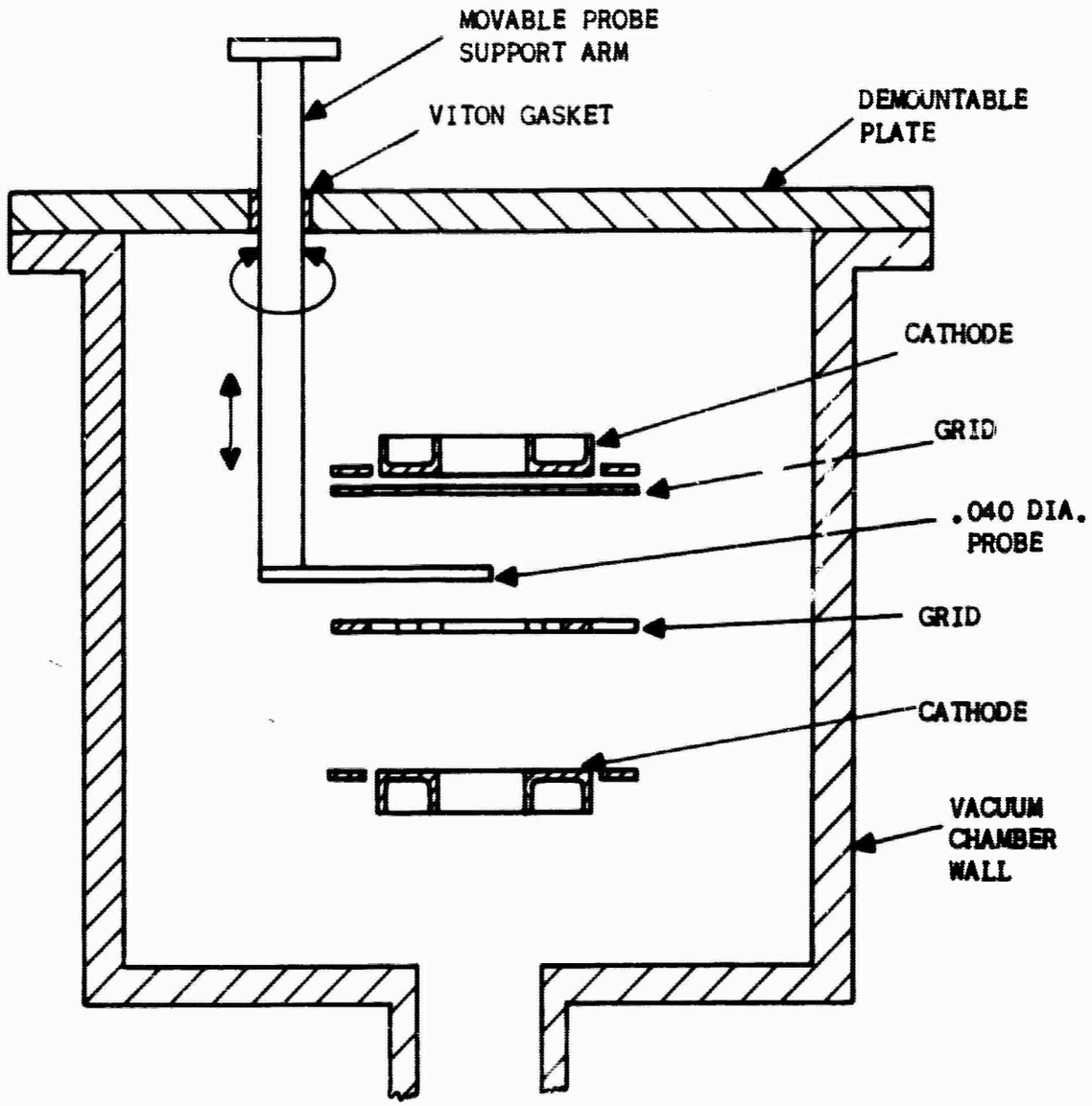

FIGURE 10

PLASMA GENERATOR ELECTRODE AND PROBE STRUCTURE

D-1398

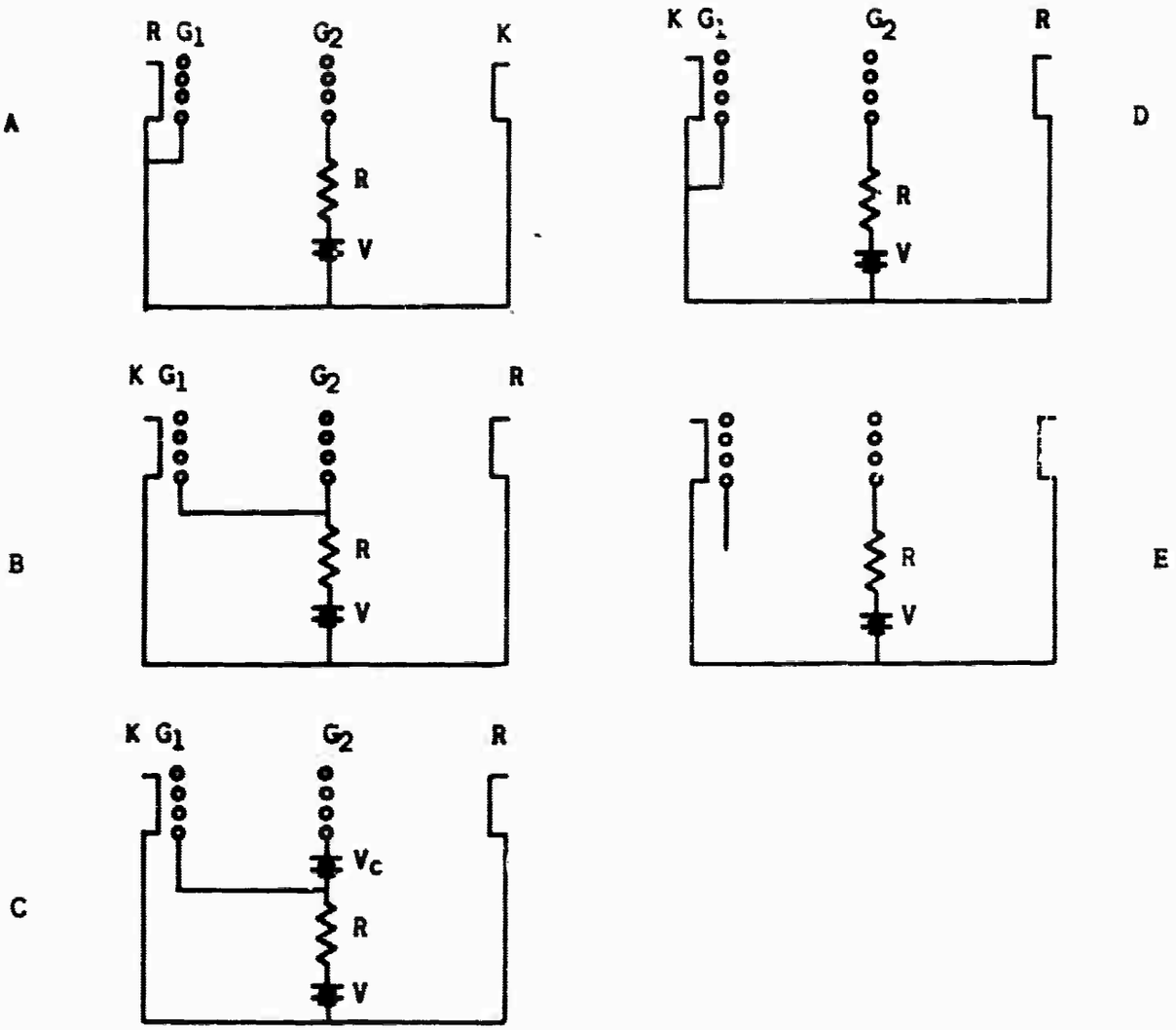

FIGURE 11

PLASMA GENERATOR TEST CIRCUITS

D-1396

(G_1, G_2). The results of this investigation of the influence of the close grid will be discussed later in the report.

Effect of Grid Configurations

In conjunction with the above change, the structure of the grid was also changed. The conventional grid which has been investigated in the previous reports is shown in Figure 12a. This grid has variable grid openings for ease of fabrication with a spot-welder. It was found in practice that spot-welding the wires was a very tedious task, and difficulty was encountered in maintaining a flat structure. To avoid these disadvantages, the grid structure, shown in Figure 12b was fabricated by means of a spark machining process. Grids made in this manner are more economical and complex planar geometries can be reproduced exactly.

The size of the grid opening was designed approximately equal to the smaller openings in the spot-welded grids of Figure 12a. This size opening was chosen because it was felt that the noise properties of the discharge were controlled mainly by the smallest diameter grid opening. However, use of the grid in Figure 12b in the tube resulted in generally unstable operation accompanied by higher voltage drops and consequently higher extinguishing pressures. Concurrent with this was a reduction in the electron density. In order to avoid this effect, the grid in Figure 12b was modified to the configuration shown in Figure 12c by removing some of the grid spaces to provide grid openings which were approximately equal to the largest openings in Figure 12a. It was felt that the harmful effects of the grid in

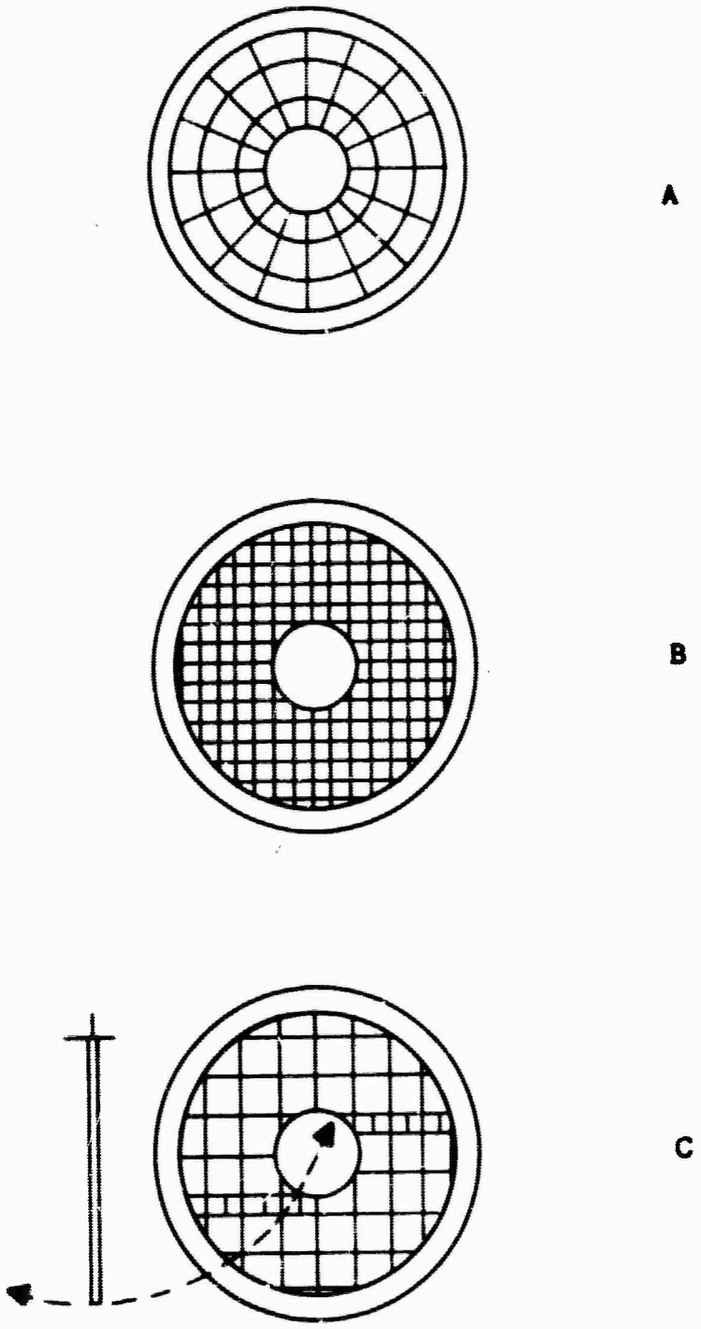

FIGURE 12

GRID CONFIGURATIONS

D-1397

Figure 12b were due to too great an interception of the electron current by the additional grid wires of the structure in Figure 12b. The results obtained with the grid in Figure 12c showed that such was the case inasmuch as extinguishing pressure and voltage drop of the tube with this type grid were comparable to tubes with grids of the type in Figure 12a. In addition, no appreciable deterioration in the noise characteristics of the discharge occurred due to the increased grid openings. On the basis of these results, it is felt that the most significant diameter relative to the control of discharge noise is probably the diameter of the inner grid circle. This diameter is controlled by the size of the electron beam. It must be large enough to permit the beam to pass without any interception by the grid.

Probe Measurements

The data presented in the previous quarterly report suggested that the electron density distribution in the plasma generator was non-uniform. In order to provide measurements throughout the entire plasma generator volume, a structure was designed so that a Langmuir probe could be moved throughout the entire plasma volume. Figure 10 shows the electrode structure inside a four inch diameter metal cylinder. A demountable top is provided to make ready changes in the electrode structure. A movable probe is inserted in the top of the housing through a Viton O ring. The probe can be moved up and down and rotated from outside of the structure. The probe movement is indicated by the arrows in Figure 10. The path followed by the probe during rotational movement is shown in Figure 12c. The volume

between the lower cathode and center grid can be probed by rotating the probe away from the grid and pushing the probe below the grid. With this type of structure, we can obtain measurements at any point along the axis and probe a certain portion of the radial variation from the center of the tube to the edge.

Initial measurements indicated that the 0.100 in. diameter probe tip was too large relative to the density variations which were occurring near the grid wires. The grid structure strongly affects the density distribution and the 0.100 in. diameter probe is too large relative to the diameter of the grid openings. To avoid this problem, the probe diameter was reduced to 0.040 in.

The results of the probe measurements are shown in Figures 13 and 14. Figure 13 shows the radial variations in electron density. For convenience in interpreting the wide variations which occurred, the cross-section of the cathode and grid is included with the graph. It is seen that the electron density peaks at the axis of the tube. The density approaches zero as the probe approaches the first solid section of the grid. As the probe moves further out in radius, another density peak occurs midway between the two solid sections of the grid wires. A minimum occurs at the next grid wire followed by another maximum in the center of the next grid opening. The density then goes to zero again as the probe approaches the edge of the grid. It is noted that the maximum within the grid openings are greater than the density maximum which occurs in the center of the tube. This is due to the presence of the cathode emitting surface directly

BLANK PAGE

FIGURE 13

RADIAL DENSITY PROFI

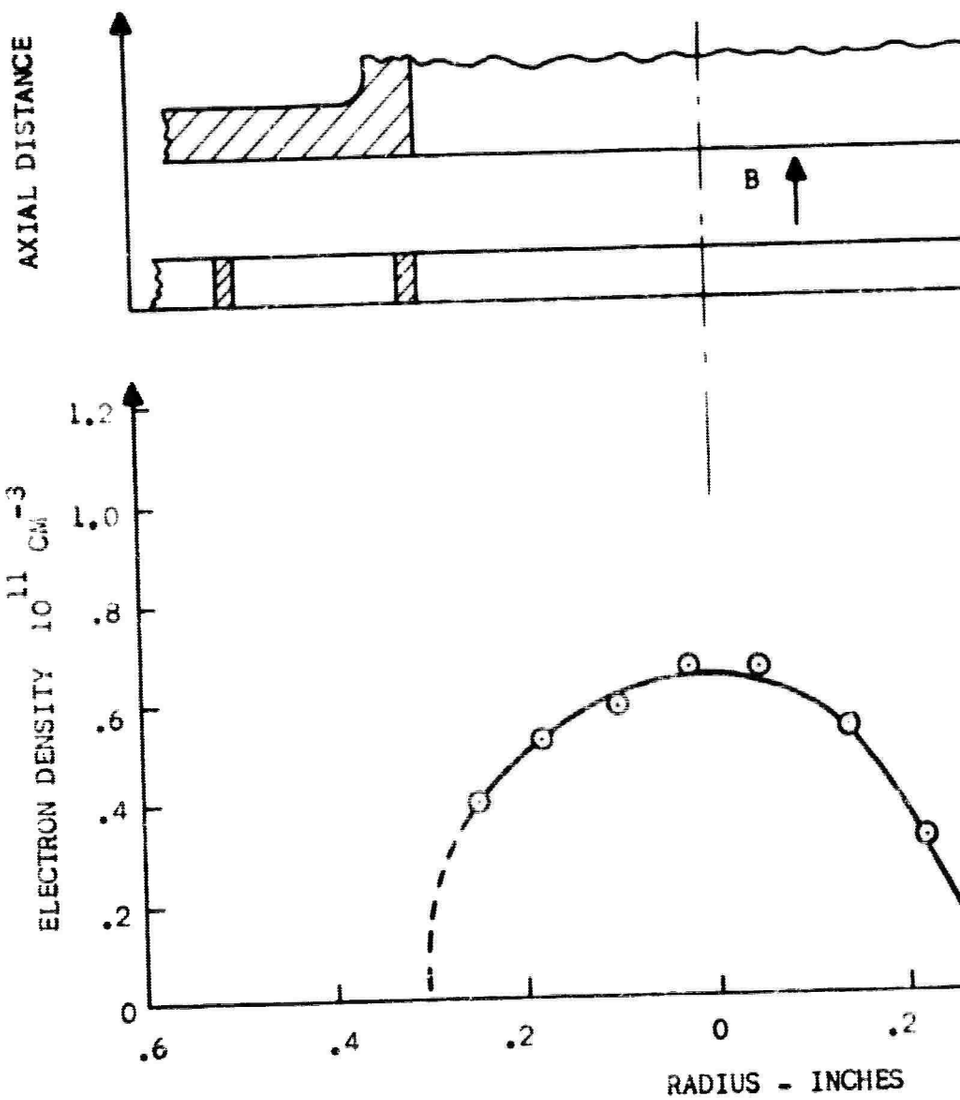

D-1394

ROFILE

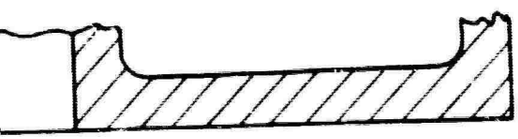

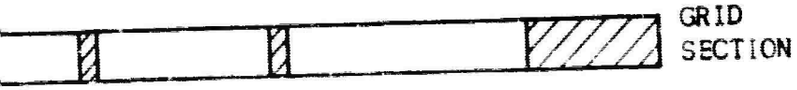

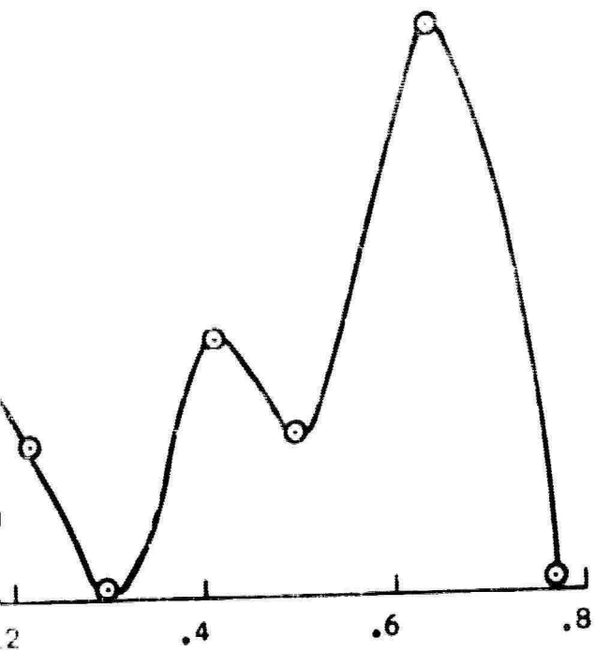

B = 300 GAUSS
I = 1200 MA

CIRCUIT B

FIGURE 14

AXIALLY DENSITY PROFILE

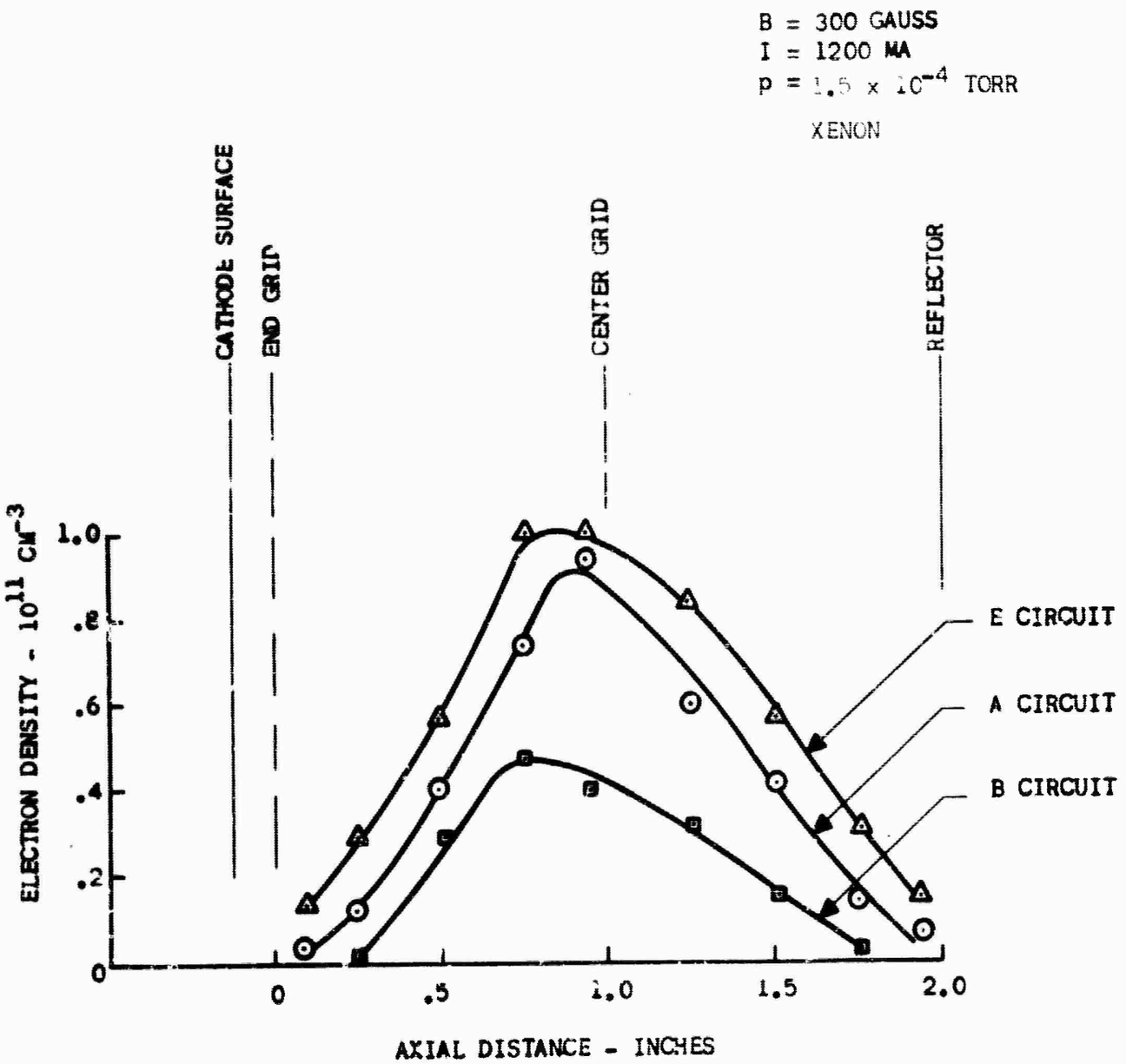

D-1395

over the grid openings. The electron density in the center of the tube is maintained by diffusion from the grid region across the magnetic field; hence, a lower electron density in the center of the tube. The magnetic field direction is shown in Figure 13 as being parallel to the axis of the tube. It is thus seen that the grid structure has a profound effect upon the radial electron density distribution. Interception by the solid grid sections reduces electron density to very low values in the cylindrical volumes generated by the solid grid sections and the magnetic field vector. This density variation is very significant relative to the coupling problem. The electromagnetic signal will encounter large density variations in traveling from outside the tube to the beam interaction region in the center of the plasma volume.

Increasing the magnetic field had little effect on density in the center of the tube or on the general radial profile. However, the peak electron density in the center of the grid openings increased with increasing field.

Axial density profiles are given in Figure 14 for three different circuits. It is seen that maximum density occurs in the center of the tube close to the center grid. The actual peak appears to be shifted in the direction of the cathode. This indicates that a fraction of the primary electrons are only available for ionizing collisions in the initial traverse between the cathode and the center grid. This portion of the primary electrons is collected at the center grid and cannot make additional ionizing collisions in the

region between the center grid and reflector. Again, it is seen that a marked electron density variation occurs with the result that the beam plasma interaction can only occur over a relatively short axial distance. For example, in the case of circuit E, the electron density is greater than $0.8 \times 10^{11}/cm^3$ over an axial distance of approximately .6 to 1.3 inches. This is a total distance of .9 inches compared to an overall cathode to reflector spacing of 2.1 inches. It is felt that this type of profile can be controlled by altering the tube geometry. For example, one possibility would be the use of additional grids. By varying the potential and current to these grids, it should be possible to alter the axial profile and obtain a more uniform axial density.

Effect of Circuit Variations

The circuits investigated are shown in Figure 11. In all cases the tube was operated with only one cathode hot. The hot cathode is designated K and the cold cathode is designated as an electron reflector R.

In circuit A the close grid (G_1) is connected to the cold cathode (R) to effectively give a three element tube consisting of cathode (K), a center grid (G_2) and a combination reflector (R and G_1). In circuits B to E the opposite cathode is hot. This was expected to result in a four element tube consisting of a cathode (K), a grid close enough to the cathode to influence emission (G_1), a center grid (G_2) and a reflector (R).

In circuit C a variable voltage source (V_c) has been connected

between the two grids. This provides all intermediate conditions between the limiting cases of circuits B and D. In circuit B the grids are tied t gether which is equivalent to setting V_c equal to zero in circuit C. In circuit D, G_1 is tied to the cathode which is equivalent to the situation which occurs in circuit C when V_c is increased to a level such that the action of the load resistor (R) decreases the voltage between G_1 and K to zero.

In circuit B, it was observed that half of the cathode current is collected by the close grid and half by the center grid. This is also true for V_c equal to zero in circuit C. Increasing V_c increases the fraction of cathode current collected by the center grid. In the extreme case of circuit D, nearly all of the cathode current is collected by the center grid and only a negligible fraction by the close grid.

The electron density was found to increase with center grid current in a manner analogous to the situation described in the previous quarterly report. Accordingly, circuit D in which all of the cathode current is collected at G_2 gives a much higher electron density than circuit B in which only half of the cathode current is collected at G_2. Measurements showed that the density with D was twice that with circuit B. This led to the conclusion that the half of the cathode current collected by G_1 in circuit B was primary electron current which made no ionizing collisions. The portion of the cathode current which is effective in producing a plasma is that which is drawn past G_1 and into the main volume of the tube where it is collected

by G_2. Such an analysis also leads to the conclusion that G_1 serves no useful purpose in controlling plasma generation in the above modes of operation. This is verified by the fact that operation with circuits in which there effectively is no close grid, resulted in an electron density which was nearly equal to that obtained for circuit D. Thus circuit A can be considered equal to circuit D. In addition, circuit E in which the close grid is left floating so that all of the cathode current must be collected by G_1, also gives electron densities comparable to A and D.

Electron density measurements obtained with the different circuits are presented in Figure 14. It is seen that axial electron density measurements for circuits A and E are approximately twice that for circuit B. The density difference between circuits A and E is attributed to the fact each circuit utilizes different hot cathodes with slightly different emission characteristics.

The above results were observed for a tube containing a high transparency type C grid shown in Figure 13. More complex behavior was observed for the lower tranparency A and B grids. In these cases, a greater interaction between G_1 and the cathode resulted in higher extinguishing pressures for all circuits except the low density B circuit. As discussed earlier, the low transparency B grid consistently gave unstable behavior and high extinguishing pressures. Use of the intermediate transparency A grid with a B circuit resulted in low extinguishing pressures comparable to those observed for the C grid with all circuits. In fact, one of the original reasons for

the introduction of an A grid near the cathode was its stabilizing influence on low pressure operation.

In summary, optimum performance is obtained in terms of low pressure operation at high electron densities and minimum discharge noise with a high transparency C grid operated in a circuit in which all of the cathode current is collected by a grid in the center of the plasma volume. Use of high transparency grids eliminates the need of extra grids near the cathode.

Effects of Different Gases

Various inert gases were investigated to determine if some gas other than xenon would give a larger pressure range between the minimum pressure at which the plasma generator will operate and the maximum pressure at which the electron beam breaks up in an amplifier tube.

Under the present state-of-the-art, the minimum pressure at which the required density of 1.1×10^{11} electrons/cm^3 can be produced is about 1.0×10^{-4} Torr. This pressure is comparable to that at which initial beam break-up occurs at about 1.8×10^{-4} Torr.

The data for the plasma generator was obtained by observing the lowest pressure at which a density of 1.1×10^{11} electrons/cm^3 can be produced under known conditions in a separate plasma generator tube. The beam break-up observations were made on tube number 2A (coupling tube) at peak beam currents of 1.5 amps. However recent data with tube number 3 with uniform field indicates that the full beam current of 2.8 amps can be obtained at xenon pressures of 1.8×10^{-4} Torr.

The data presented in Table II gives both absolute pressure readings

TABLE II

Gas	Pressure - Torr		
	Plasma Generator	Initial Beam Break-up	Complete Beam Break-up
Xenon	1.0×10^{-4}	0.10×10^{-4}	0.5×10^{-4}
Argon	4.2	0.36	3.4
Neon	27.	2.6	24
Helium	120.	28.2	125

Gas	Pressure Ratio (P/P_{xenon})		
	Plasma Generator	Initial Beam Breakup	Complete Beam Breakup
Xenon	1.0	1.0	1.0
Argon	4.2	3.6	6.8
Neon	27.	26.	48
Helium	120	282	250

and pressure ratios relative to xenon. Because of the reasons discussed above, the beam break-up pressures are lower than that at which the plasma generator can be operated. Accordingly, use of pressure ratios provides a means for comparing plasma generator operations with beam break-up performance.

The data shows that no appreciable initial beam break-up improvement can be obtained by using argon or neon because the pressure ratio increase for these gases is comparable to the increase for plasma generator operation. The initial beam break-up pressure ratio for helium of 282 is more than twice the plasma generator pressure ratio of 120 for helium. Improved performance might thus be obtained with helium; however, high voltage drops and slightly unstable operation with this gas will require further investigation.

Argon, neon, and helium all show higher complete beam break-up pressure ratio increases than the corresponding ratios for plasma generator operation. This indicates an apparent increased pressure range between minimum plasma generator pressure and maximum complete beam break-up pressure, but again higher voltage drops and slightly unstable operation with these gases will require further investigation.

Cesium Plasma Generator

During this period work was continued on the task of generating a low pressure thermally ionized cesium plasma to provide an alternate approach to the problem of electron beam break-up. The cesium plasma generator test vehicle shown in schematic form in Figure 15 and in detail in Figure 16 has been fabricated using design principles

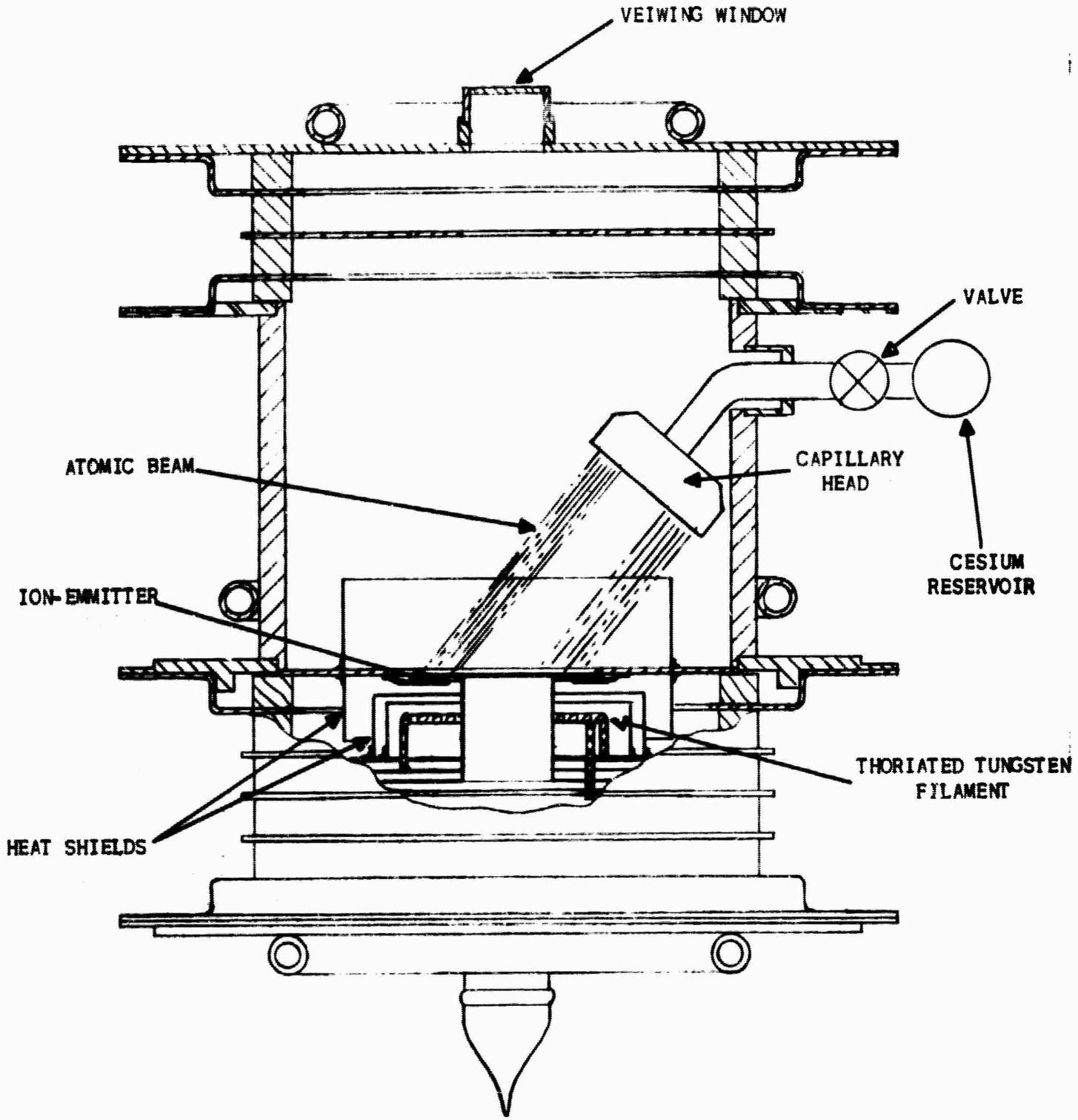

FIGURE 15

CESIUM PLASMA GENERATOR

-1163

BLANK PAGE

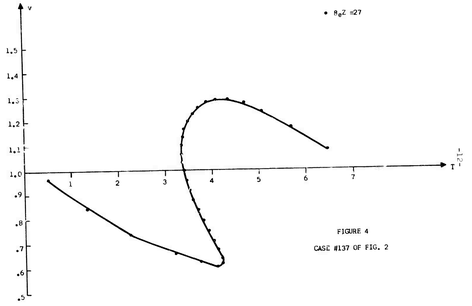

FIGURE 4
CASE #137 OF FIG. 2

D-1440

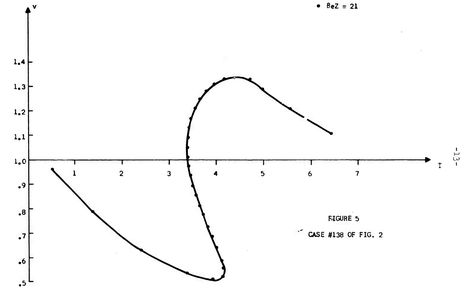

FIGURE 5
CASE #138 OF FIG. 2

D-1438

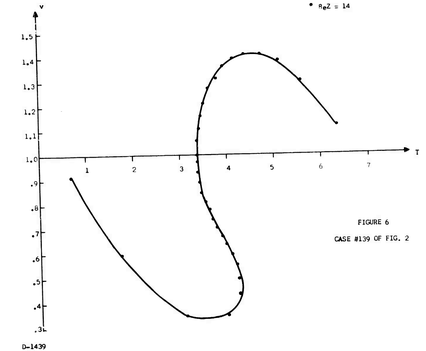

FIGURE 6
CASE #139 OF FIG. 2

D-1439

up into a maximum o
plasma density and
practical plasma ge
mental tubes, axial
and indeed are desi
thus necessary to i
with axially non-u
ted in Figure 7 the
lower density regio
frequency f, the ra
the plasma. For th
beam current of ove
that, at the point
the electrons close
dc velocity indicat
It is noted from Fi
with distance from
region indicating t
ent operation is o

Efficiency Consider

In calculating
include the magnitu
swing at the output
coupler[1].

1. S. E. Webber, "
Klystron," I.R.

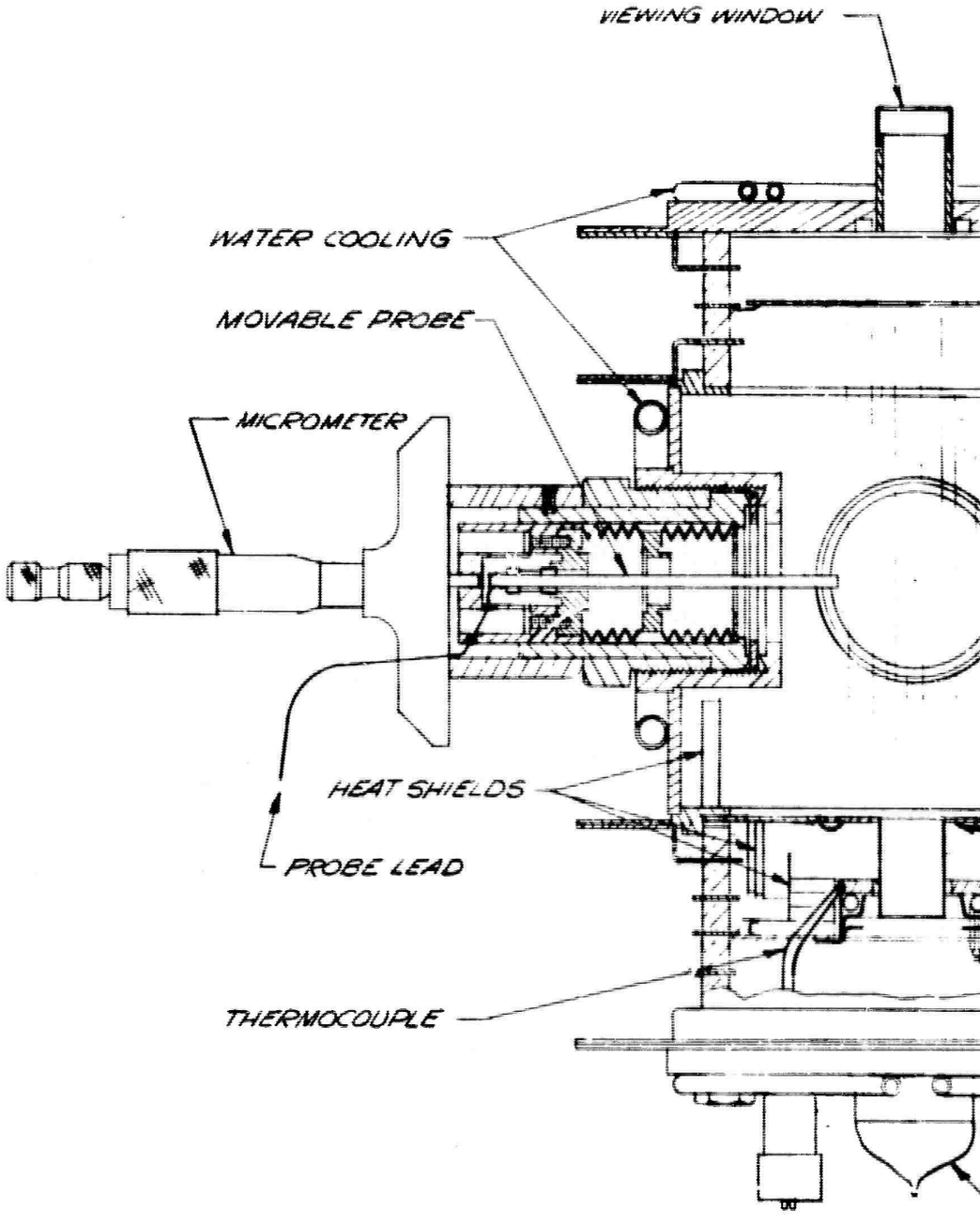

FIGURE 16
DETAIL OF CESIUM PLASMA TESTE

D-1443

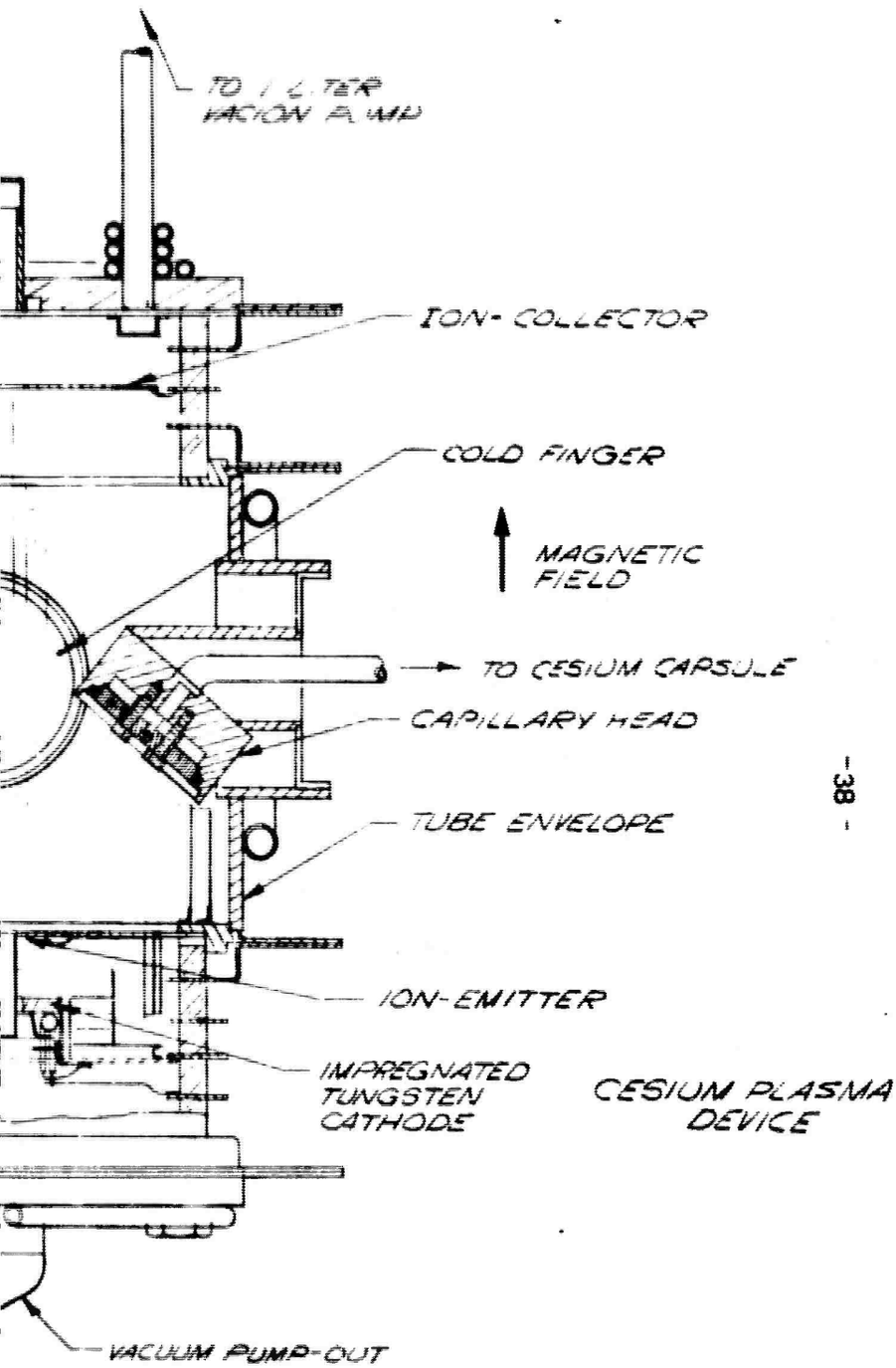

CESIUM PLASMA DEVICE

ESTER

discussed in the previous quarterly report. The detailed drawing in Figure 16 includes a movable probe for measuring electron density and a cold finger for condensing unionized cesium. The test vehicle is ready for final testing. Because of the complexity of the device, preliminary tests were run to independently check the design of the cesium atomic beam forming sections and the ion emitter section.

The cesium atomic beam forming section was tested by replacing the ion emitter section with a water cooled glass plate. A uniform deposit of cesium condensed on the cool glass plate indicating that a uniform atomic beam was produced.

Two different methods of electron bombardment for heating the ion-emitter to the required 2000°K operating temperature were investigated. One method utilized a directly heated thoriated tungsten filament as shown in Figure 16 as an electron source. In the second method, an indirectly heated tungsten matrix cathode was used.

An ion-emitter assembly with a thoriated tungsten filament was operated separately in a vacuum bell jar. Unfortunately, the high operating temperature of the filaments produced excessive out-gassing of the surrounding ion emitter assembly which poisoned the thoriated tungsten. From the experience gained during this particular test, it is felt that the thoriated tungsten approach can be made to work although additional experiments must be performed to provide better outgassing control.

At the present time, the tungsten matrix cathode approach appears more promising. This type cathode is less susceptible to poisoning

because free barium is constantly diffusing to the surface from within the bulk of the material. An initial test was run by enclosing an ion-emitter assembly with a tungsten matrix cathode in a glass envelope. This test was inconclusive because inadequate heat shielding raised the glass walls to temperatures near the glass melting point. Another test is presently in progress in which the tungsten matrix cathode is being evaluated directly in the cesium plasma generator in Figure 16. During this evaluation, the atomic beam forming section will not be in operation.

V. AMPLIFIER TEST RESULTS

During this quarter, testing of the second coupling vehicle, tube 2A, was completed. This tube was described in detail in the Fourth Quarterly Report. Figure 17, a layout of the tube, is repeated here for convenience. As discussed in the last report, it was not possible to obtain full beam current and a stable plasma simultaneously. Therefore, all the data discussed below was obtained with reduced beam current.

Data reported last quarter from this tube indicated 15 db of waveguide coupling enhancement due to the presence of the plasma. Since this enhancement was always accompanied by approximately 30 db of cavity-to-cavity gain, it was not possible to separate the gain from the coupling improvement to determine the exact amount of coupling.

The method used for obtaining this data was to adjust the tube for maximum cavity gain and then to measure the waveguide output. This was done to insure that the proper plasma density had been achieved. Since the coupling waveguide extended through the tube, it was possible to check the plasma density by microwave scattering measurements on the plasma without the use of the beam. To do this, a microwave signal is introduced into one side of the waveguide and a detector is placed on the other. The transmission properties of the plasma can then be measured as a function of discharge current, magnetic field, pressure, and frequency. Resonances which are indicated by a dip in transmitted power can then be plotted.

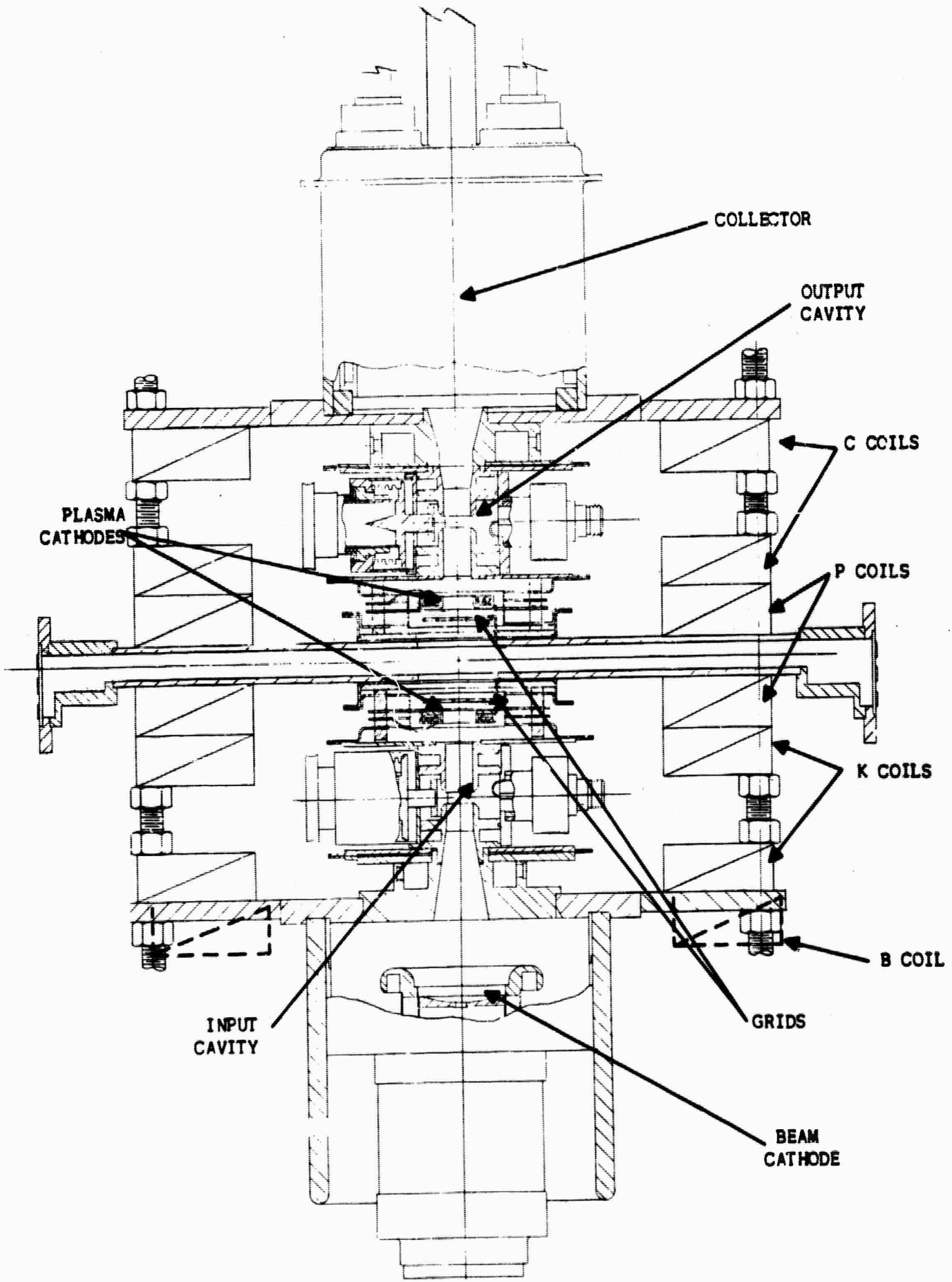

FIGURE 17
TUBE 2A

D-1154

The results of this experiment proved very interesting. Under the conditions which produced the maximum cavity-to-cavity gain, no resonances could be found, although the high values of this gain were positive proof that the proper plasma density existed. However, if the magnetic field was increased to values much higher than those required for gain, a series of resonances could be observed. Figure 18 is a typical plot of these resonances.

With the discovery of this phenomena, the amplifier circuity was set up as before; that is, the microwave signal was introduced into the input cavity and the output of the waveguide and output cavity signals measured with the beam on. The unused waveguide output was terminated with a movable short. Figure 19 is a schematic drawing of this set up. The waveguide and cavity gain were then measured under the conditions which had produced resonances with the scattering measurements.

Waveguide gain improvements of over 15 db were again observed when the plasma discharge current corresponded to that for a scattering resonance, however, the cavity gain showed little change over that with no plasma. Figure 20 is a typical plot of waveguide and cavity gain versus discharge current. Since the cavity output showed no significant increase due to the plasma, it can be concluded that there was little plasma gain and that the increase in waveguide output was caused entirely by coupling enhancement due to the plasma. The horizontal line in Figure 20 indicates the coupling achieved in tube number 2 discussed in the last report. In this tube the waveguide hole

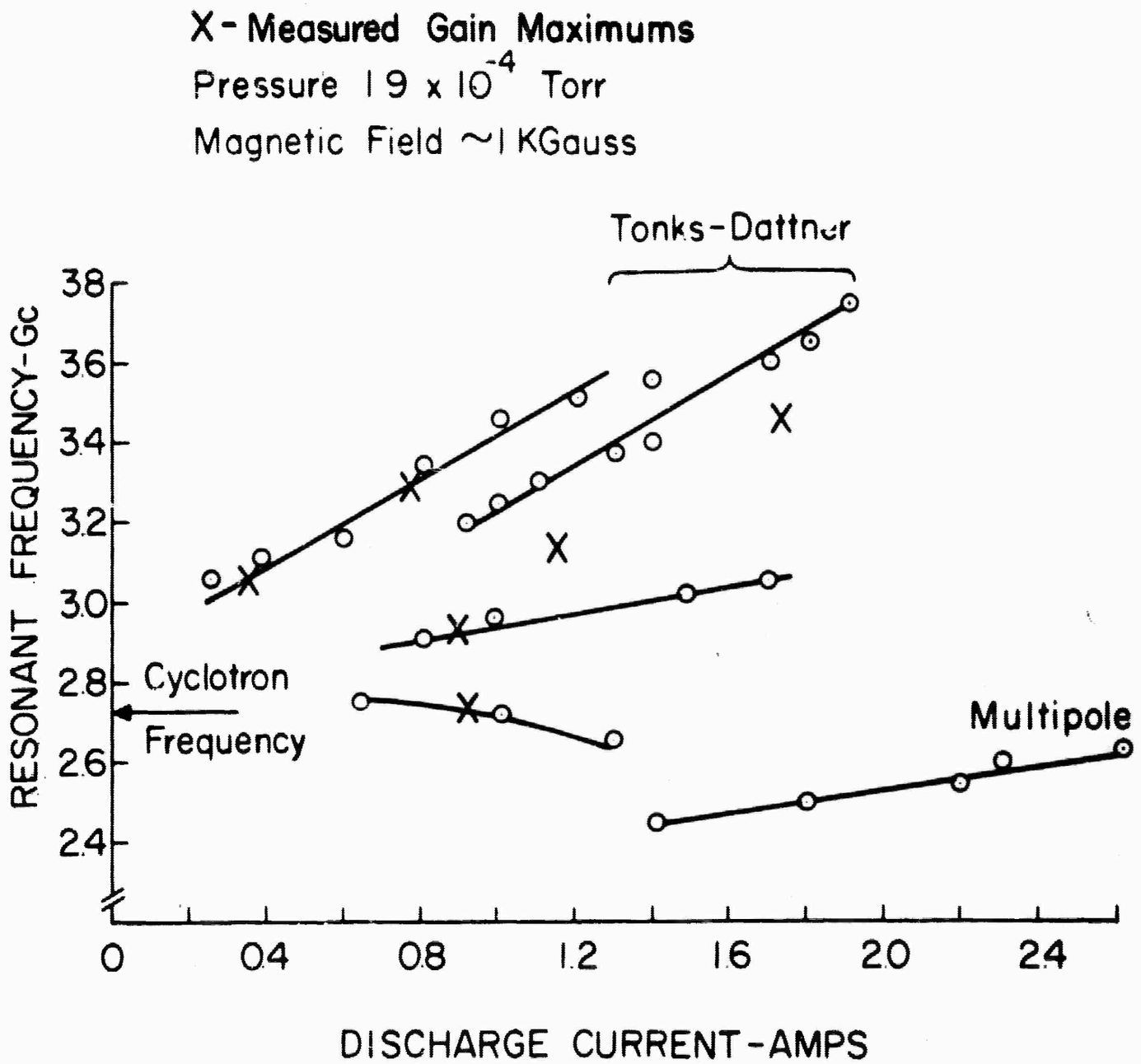

FIGURE 18

PLASMA RESONANCES

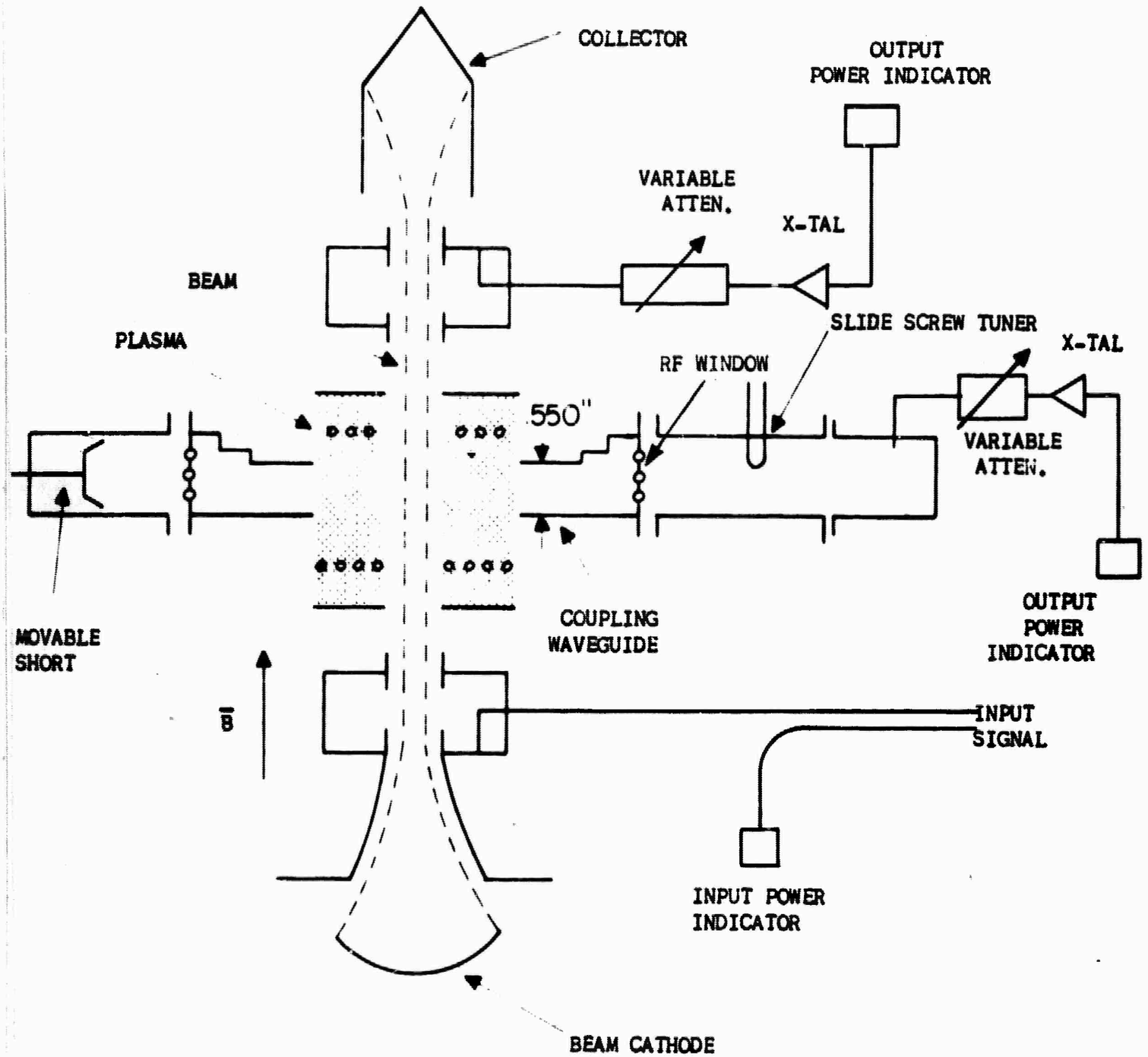

FIGURE 19

SCHEMATIC DRAWING OF GAIN MEASUREMENT EXPERIMENT

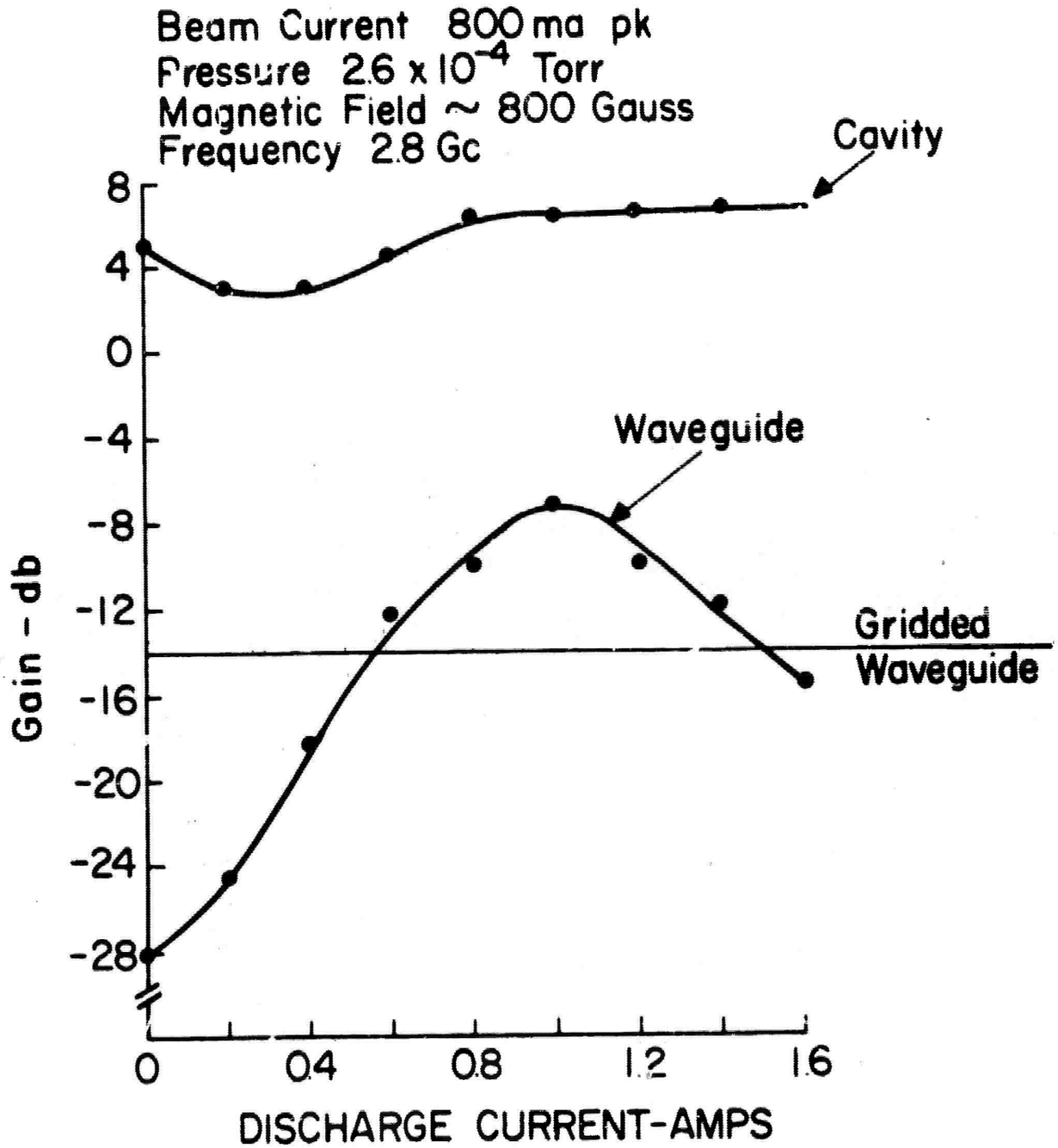

FIGURE 20

GAIN VS. DISCHARGE CURRENT

was gridded such that the beam was more tightly coupled to the waveguide. From this it can be seen that the plasma more than compensates for the removal of the grids from the waveguide hole.

An explanation of the observed phenomena may lie in the radial density variation of the plasma. As noted in Section IV above, Langmuir probe measurements made on the plasma tester indicate that the plasma is denser in the region directly over the plasma cathode than on the axis.

Since maximum cavity gain would require that the plasma have the proper density on the axis, the density outside the beam would be too high for optimum coupling to the waveguide. The scattering measurements, on the other hand, actually look at the density of the outside of the plasma and therefore, will indicate when the plasma in the annular area around the beam is the proper density. A cross-sectional view of the coupling region is shown schematically in Figure 21. This indicates the annular nature of the plasma and shows the relation between the waveguide, plasma, and beam.

The scattering measurements indicated a multiplicity of resonances as indicated in Figure 18. Several authors[2,3] have discussed this affect and the present consensus is that the finite geometry and radial non-uniformity are the cause. The behavior of the resonances suggests the labeling used in Figure 18 after Crawford[3]. Waveguide gain maxima were observed that corresponded to the several resonances. The value

2. J. C. Nickel, J. V. Parker, and R. W. Gould, Phys. Rev. Letters 11, 183 (1963).
3. F. W. Crawford, Resonances of a Cylindrical Plasma Column (Stanford University Microwave Laboratory Report No. 1045, Stanford 1963).

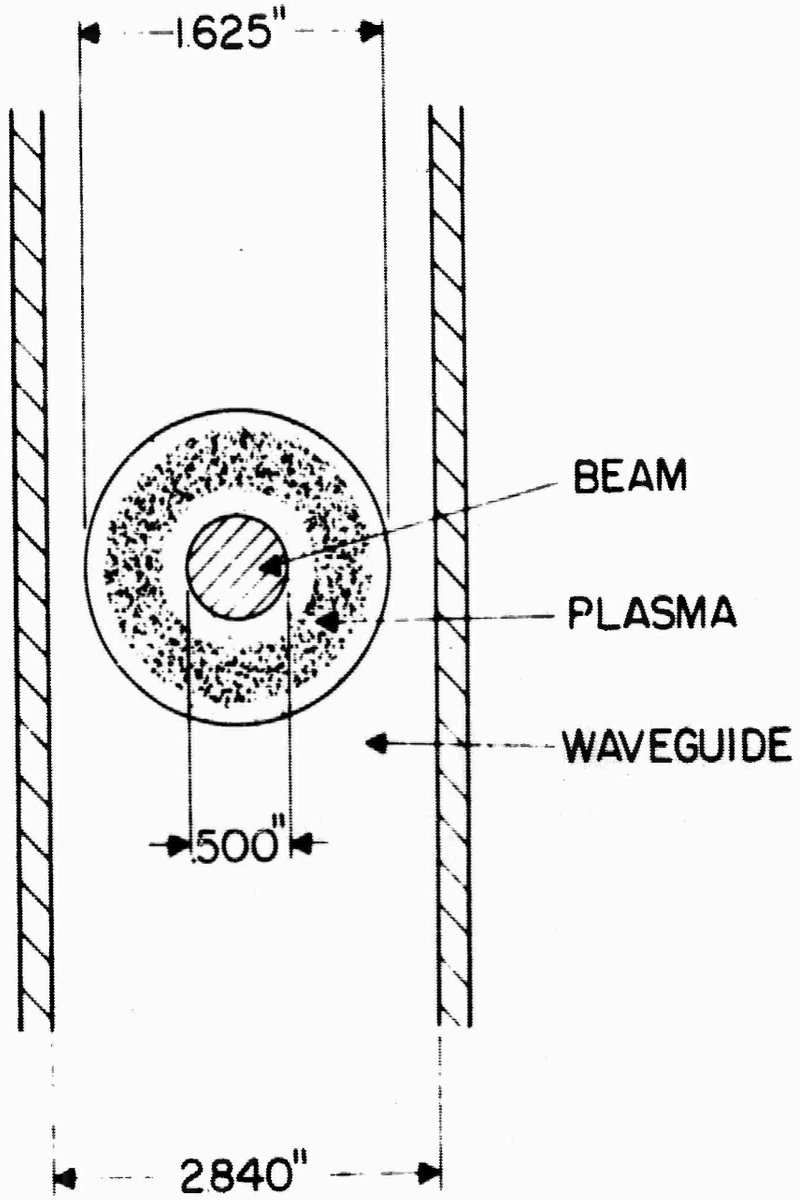

FIGURE 21

CROSS SECTION OF COUPLING REGION

of resonant discharge current for the highest frequency mode observed agreed exactly within experimental error with the current at which the waveguide gain maximized. Agreement with the other modes was not as good. This is shown by the experimental points plotted in Figure 18.

Of particular interest was the waveguide gain at the cyclotron resonance. An oscillograph of the waveguide output at that point is shown in Figure 22. The output is free of the characteristic low frequency noise usually seen on plasma devices. As seen from Figure 18 the response is only weakly dependent on the discharge current, i.e., plasma density. This indicates that the low frequency noise on the outputs at the other resonances is caused by plasma density fluctuations.

The bandwidth of the coupling interaction was measured by changing the signal frequency and tuning both the input cavity and the sliding waveguide short at each frequency while the beam and plasma parameters were held fixed. Figure 23 is a plot of these results which is typical of the many cases run. The coupling bandwidth was consistently in the order of 100 Mc to the 3 db points. As the cavity-to-cavity gain bandwidth reported last quarter is much larger, this indicates a geometrical dependence. It is felt at the present that proper external circuity close to the plasma will greatly increase the coupling bandwidth as will a more uniform plasma.

The results of the experiments on tube 2A show that the presence of a plasma between the beam and the metal circuity can greatly increase the coupling. The radial density variation in the plasma which

FIGURE 22

OUTPUT PULSE AT CYCLOTRON RESONANCE

MAGNETIC FIELD 1 K gauss
FREQUENCY 2700 mc

PEAK BEAM VOLTAGE 20 KV
PEAK COLLECTOR CURRENT 0.55 AMP

GAS-XENON

PRESSURE 2×10^{-4} torr
DISCHARGE CURRENT 1.2 A

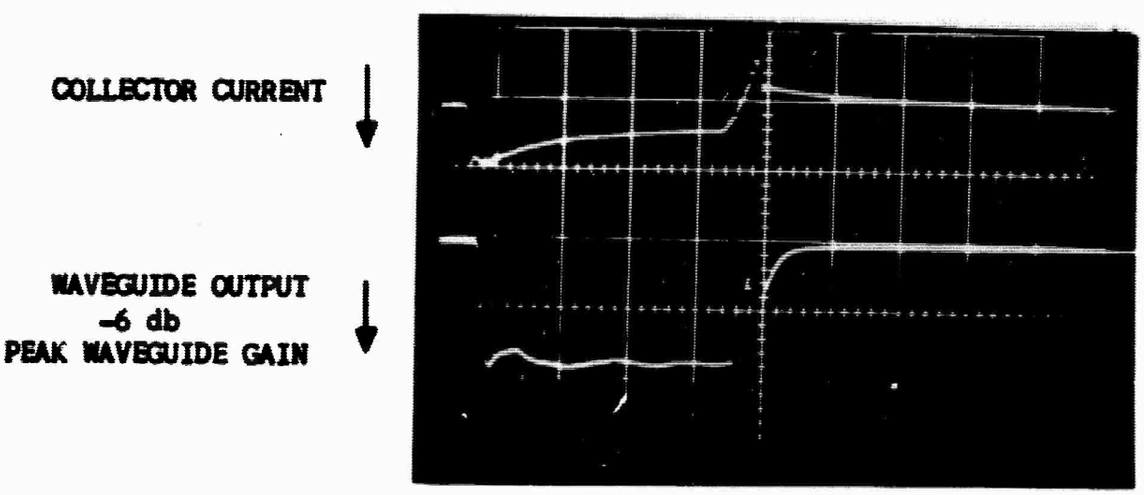

FIGURE 23

COUPLING
BANDWIDTH

PRESSURE 2.6×10^{-4} TORR
GAS XENON
PEAK BEAM CURRENT 20 KV
PEAK COLLECTOR CURRENT 0.55 AMPS
PLASMA CURRENT 1.0 AMP

* MAGNETIC FIELD

COLLECTOR COIL CURRENT 8.0 AMPS
PLASMA COIL CURRENT 8.0 AMPS
CATHODE COIL CURRENT 8.0 AMPS
BUCKER COIL CURRENT -1.5 AMPS

* REFER TO FIG. 17

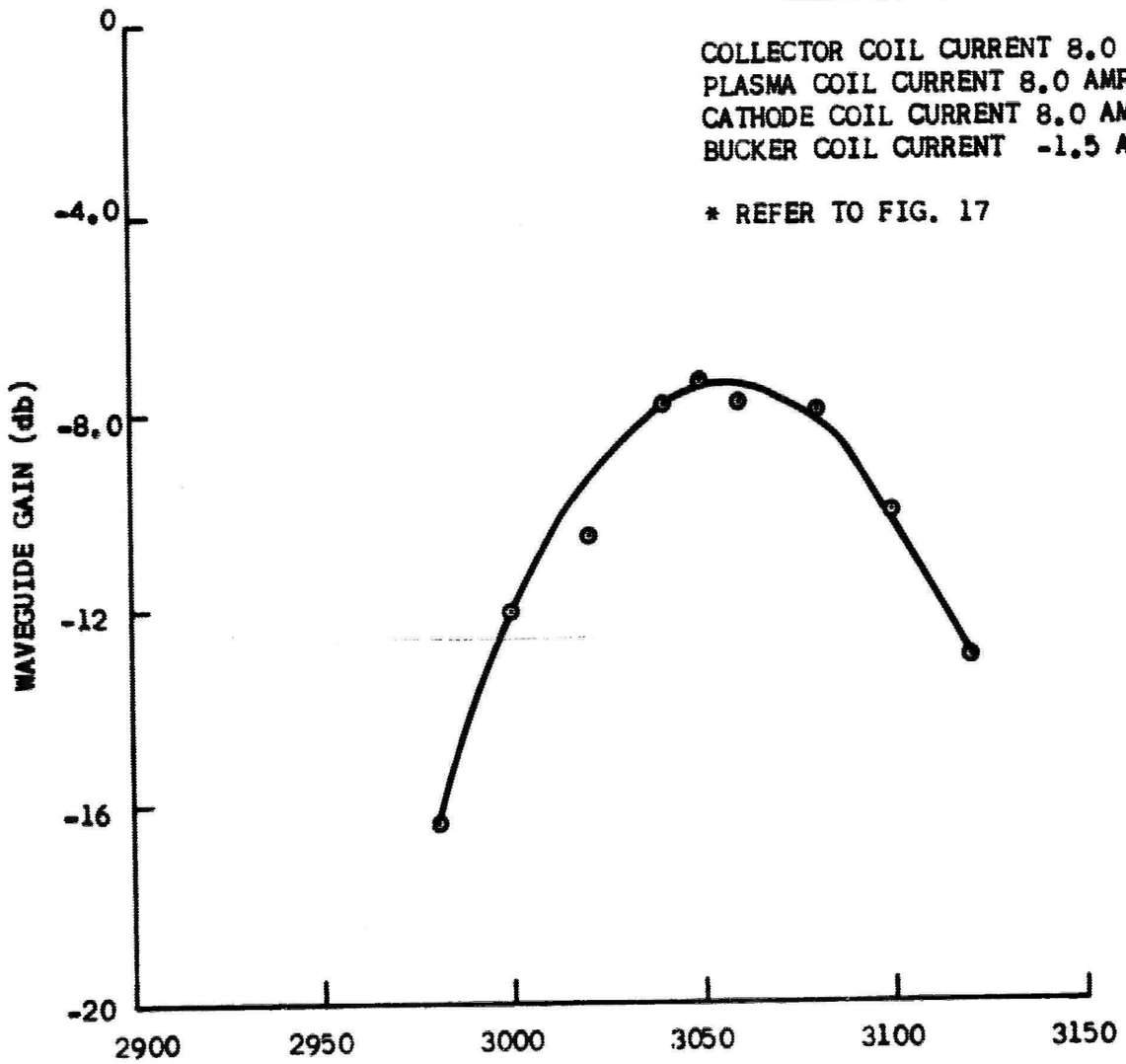

would not allow high gains and high coupling simultaneously with this tube will not present a difficulty in an amplifier tube. Since the plasma has an axial variation along with the radial variation, discussed in Section IV, it is merely required that the couplers be placed in the proper axial position to achieve gain and coupling simultaneously.

Since testing of tube 2A had shown cavity-to-cavity gains greater than 30 db, it was decided to rebuild tube number 1 with a plasma generator of better design. This tube is designated tube number 3, and shown in detail in Figure 24.

The recent work on plasma generation had shown that suitable plasmas could be achieved at pressures near 1×10^{-4} Torr. On tube 2A, full beams could be achieved with no beam breakup at about $.6 \times 10^{-4}$. Since it would be possible to add auxiliary electrodes close to the beam to sweep away the beam formed ions, it appeared possible to raise this limiting pressure on beam operation. Such an electrode was added to tube number 3 as is shown in Figure 24. The plasma section incorporated in this tube was similar to the best design tested in the plasma tester. Since these plasma tests had shown that a uniform field is advantageous to low pressure plasma generation, no internal magnetic pole pieces were used. The plasma cathode material was a high porosity tungsten impregnate designated S-80. This material, purchased from Semicon Associates, had proved satisfactory in the plasma testers.

This tube was completely constructed and preliminary testing

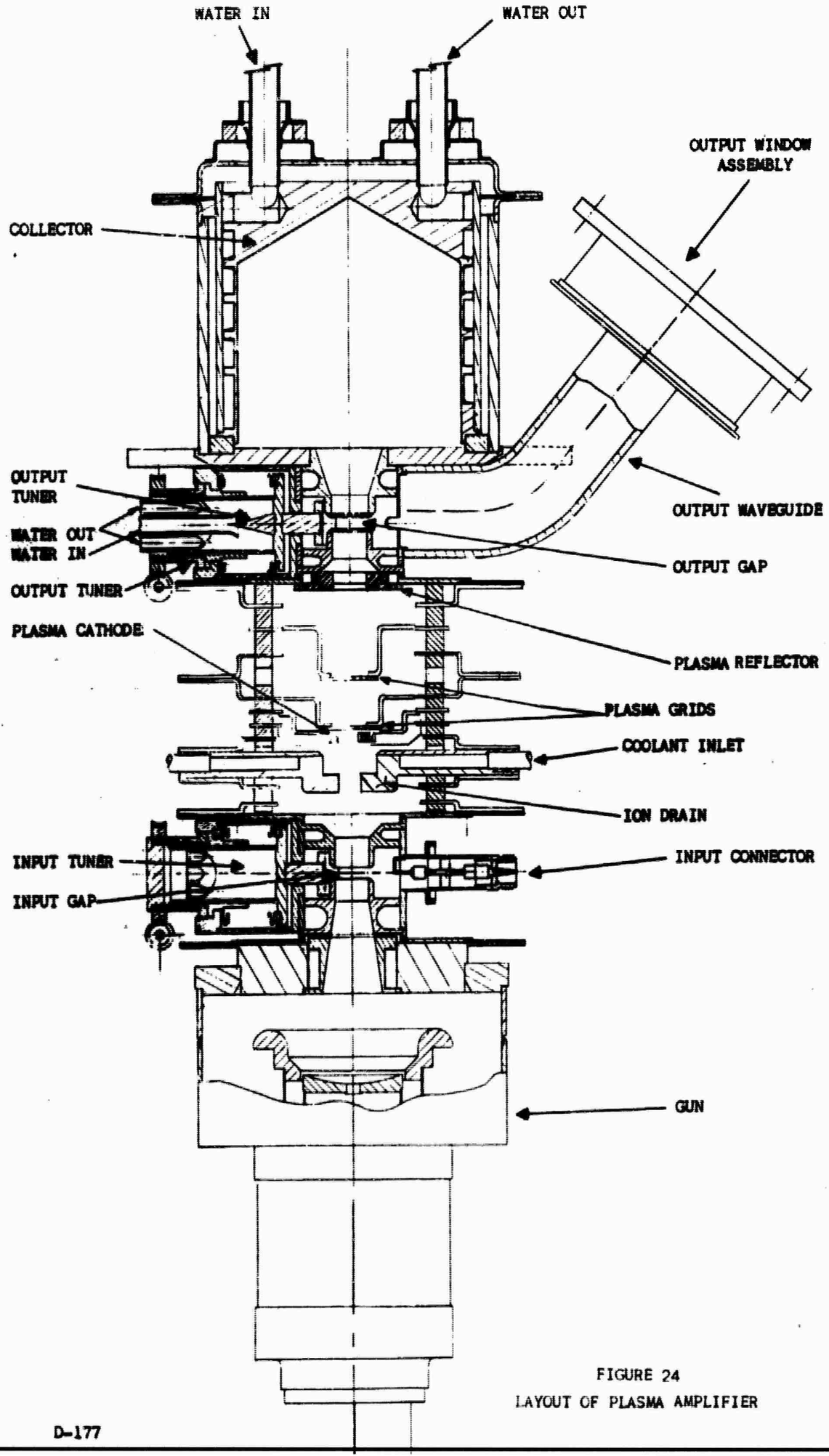

FIGURE 24
LAYOUT OF PLASMA AMPLIFIER

started during this quarter. Two results of importance were immediately noted.

1) The maximum pressure for full beam operation was much higher than expected. Quiet beam operation at pressures as high as 1.8×10^{-4} Torr were observed. This was due more to the uniform magnetic field than to the ion drain, however, the ion drain relieved the cavity de-tuning problem somewhat. Since more data will be available a discussion of these effects will be presented next quarter.

2) The minimum pressure for plasma operation was not as low as in the plasma tester. Plasma operation was complicated by the evaporation of barium from the cathode. The barium condensed on the insulating ceramic causing a short in a matter of minutes. This could be removed by applying heat to the ceramic, however, plasma measurements were impossible due to the changing resistance.

Several attempts to obtain the expected performance from the plasma section failed and it was decided to rebuild this section. The tube has been modified by replacing the cathode with a less porous material, S-84, and by placing a sputter shield over the affected ceramic. To date, no testing has been done on this modified tube.

VI. THE MODULATOR

Operation of the modulator during this quarter was completely satisfactory. During the down-time between tubes, the repaired crowbar circuit was installed. Operation with the crowbar again proved to be impossible as the rapid rise and fall time of the pulse would fire the crowbar at 7 kv. Discussions with the manufacturer, Manson Laboratories, have uncovered an incompatiability between the crowbar and the modulator. Manson has agreed to correct the situation by modification of the crowbar, and assume the responsibility for the expense of the modifications and re-installation. At this time, no further action has been taken, however, Manson has promised satisfactory operation before the end of the next quarter.

VII. CONCLUSIONS

From the large signal computer theory it can be seen that positioning of the plasma is of great importance when cavity couplers are being used. Under the proper conditions efficiencies close to 70% should be possible with well designed cavities. The application of these results to the case where plasma couplers are used is, as yet, not clear.

The measurements on the plasma probing vehicle indicate that the anode grid wires do effect the plasma density. The maximum use of discharge current is achieved by using the minimum number of grid wires required for stability.

These measurements also show the annular nature of the plasma. Thus, if the same plasma is used for gain and coupling the axial variation must be used to allow the couplers and the beam to see the same plasma density.

The coupling experiment verified the radial density variation. These results showed that the plasma does indeed enhance the coupling and that simple transverse coupling may be a fruitful approach for the final tube design.

The application of a uniform magnetic field in tube number 3 has increased the pressure at which the beam breaks up to such a point that a small pressure range exists in which operation of both the beam and the plasma is satisfactory. It is hoped that the modifications to the tube will allow further study of this effect.

VIII. PROGRAM FOR NEXT QUARTER

Continue small signal theoretical work.

Continue computer study of large signal behavior.

Continue plasma density mapping to arrive at optimum plasma geometry for low pressure operation.

Start testing of thermally ionized cesium plasma.

Continue testing of amplifier tube, number 3, with special emphasis on experimental investigation of large signal effects.

Start design of an amplifier using plasma couplers.

IX. IDENTIFICATION OF PERSONNEL

This section contains a list of key technical personnel assigned to the contract and taking part in the work covered by this report. The approximate man hours of work performed on the contract by each of the people listed are given.

M. A. Allen	129
C. S. Biechler	405
P. Chorney	37
O. Cunningham	407
H. S. Maddix	230